Spectroscopy, modeling and investigation of thulium doped tellurite glass.

Taher, Masaud Abdusalam

S/D

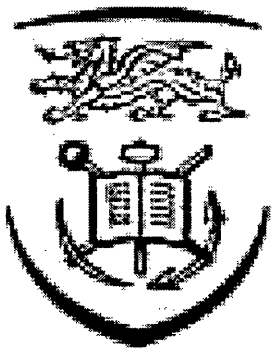

SWANSEA UNIVERSITY

SPECTROSCOPY, MODELING AND INVESTIGATION OF THULIUM DOPED TELLURITE GLASS

by

Masaud Abdusalam Taher

Submitted for the degree of Doctor of Philosophy

Multidisciplinary Nanotechnology Centre

College of Engineering

Swansea University

2011

This thesis is dedicated to my wife Rokaia Mohammed for her great support

ACKNOWLEDGMENT

I would like to thank the staff in the School of Engineering at Swansea University for their help and friendship. I wish also to thank my colleagues for their helpful assistances.

I would like to extend an extremely grateful and huge thank to my supervisor Professor Stefano Taccheo for all his patient, wisdom, and support throughout my PhD studies.

Abstract

A thulium (Tm^{3+}) doped tellurite glass with a composition $75TeO_2$-$20ZnO$-$5Na_2O$ (mol %) has been investigated. Two attractive emission transitions at 1470 nm and 1810nm were absorbed and the radiative lifetimes are 0.37 ms and 2.64 ms respectively. The 1470 nm fluorescence is broad with a full width at half maximum of 105 nm. The emission spectra achieved under 785 nm excitation reveal the existence of energy transfer via cross relaxationTm^{3+}. As a result, the intensity of the 1470 nm transition band decreases in relation to that of emission at 1810 nm, as thulium concentration increases. Anew technique was applied to calculate cross relaxation $^3H_4$, $^3H_6 \rightarrow {}^3F_4$, $^3F_4$ utilizing emission spectra has been proposed. Obtained values of cross relaxation showed linear dependence with dopant concentration and good agreement with the cross relaxation parameter extracted from lifetime measurements. Thulium energy level rate equations involving pumping rate, cross relaxation parameter and lifetimes for both levels $^3H_4$ and $^3F_4$ have been solved and the results compared with the expel data. Excellent agreement is found between simulated and experimental data, which indicates the validity of the approach.

Structure of the thesis

The structure of the work implemented in this study will be divided into five chapters. The first chapter will contain an introduction in which will state about different applications of using ~ 2 micron laser source. In this chapter, it will be explained why using thulium as active ion and why using tellurite glass as a host material.

Chapter 2 will outline reviewed topics supporting the following chapters. It will be followed by the investigation of structure and features of tellurite glasses, microscopic and macroscopic energy transfer processes, characteristics of the active ions, methods of measurements the lifetime and radiative transitions theories.

Chapter 3 will contain the laser modelling procedure. It will start with a choice of pump wavelength, followed by a rate equation system, which used in the model. In this chapter, two approaches to calculate cross relaxation parameter will be explained. Simulation and fitting will be reported as well.

In chapter 4, the thulium doped tellurite glass will be analysed. Absorption and emission spectra measurements, lifetime measurements and cross relaxation mechanism will be pointed out.

Finally, chapter 5 will present a summary of the investigation carried out summing up the conclusions.

LIST OF FIGURES

LIST OF TABLES

Symbols and Abbreviations

Symbols:

Tm^{3+}	Thulium
Ho^{3+}	Holmium
T_g	Glass transition temperature
T_x	Glass crystallization temperature
n	Refractive index
TeO_2	Tellurium oxide
Er^{3+}	Erbium
Yb^{3+}	Ytterbium
ΔT	Glass thermal stability
Li	Lithium
Na	Sodium
Mg	Magnesium
Ca	Calcium
Ba	Barium
Zn	Zinc
P(R)	Resonant energy transfer
σ_a	Absorption cross section
σ_e	Emission cross section
R	Distance between two ions
τ	Lifetime
τ_a	Acceptor lifetime
τ_s	Sensitizer lifetime
ΔE	Energy gap between two levels
N	Number of phonons
$\hbar\omega$	phonon energy
W_{mp}	Multi-phonon rate
α	Absorption coefficient
R_0	Critical transfer distance

S	Multi-polar parameter
Γ	Gamma function
N_A	Acceptor concentration
W_p	Pumping rate
A_{ij}	Radiative transition rate
τ_{rad}	Radiative lifetime
R_Q	Quenching rate
C_{SS}	Transfer constant within sensitizers
C_{SA}	Transfer constant between sensitizer and activator
η	Quantum efficiency
B	Branching ratio
F_P	Pump photon flux
P_p	Pump power
h	Plank constant

Abbreviations:

MP	Multi-phonon relaxation
ESA	Excited state absorption
ETU	Up-conversion energy transfer
NIR	Near infrared
FWHM	Full width at half maximum
LIDAR	Light detection and ranging
DIAL	Differential absorption
RADAR	Radio detection and ranging
CR	Cross relaxation
S-band	Short band
MIR	Mid-infrared
IR	Infrared
ET	Energy transfer

Contents

Chapter I

Introduction

Most of what we know about lasers and optical amplification comes from studying the interaction of electromagnetic radiation and matter, which makes spectroscopy a fundamental technique in understanding some related processes. Rare earth ions doped glass materials are the applications in which the interaction of light and matter can be considered. The spectroscopy of rare earth element doped glass material is of great interest for many science researches. Therefore, a comprehensive investigation on Tm^{3+} (thulium) doped glass material spectroscopy was carried out in this thesis. Studying spectroscopic properties of the Tm^{3+} doped glass material can contribute to the improvement of behaviour of some photonics devices performance and designs.

Extensive investigations of infrared lasers have been conducted in many laser fields, where various lanthanide dopants and host materials have been developed to target optical amplification in the infrared wavelength region. Infrared laser at wavelength region from 2 μm to 12 μm find big interest. This region offers a wide range of applications include remote sensing, medicine, and earth, atmosphere and ocean observation[1].

Remote sensing is one of various techniques that used to collect and measure optical properties. Thus, x-radiation, earth and atmospheric observation, and magnetic resonance imaging are all examples of remote sensing. Light detection and ranging (LIDAR) , one of the most known technology employed in remote sensing that measures properties of scattered light. This technique is similar to radar (Radio Detection and Ranging), however the main difference between them is that LIDAR uses much shorter wavelengths of the electromagnetic spectrum. Another important remote sensing application is for using Doppler Radar for monitoring of speed limits such as wind speed [2,3]. Remote sensing can divided into types: passive and active remote sensing. The passive sensors detect the radiations that are emitted or reflected by the object. Examples of this kind of sensors include radiometers, infrared, and film photography. On the other hand, the active sensors emit energy in order to scan objects then detect and measure the radiation that is reflected from the target. RADR

is an example of active remote sensing. Light detection and ranging as application of remote sensing data is used to detect and measure the concentration of different chemicals in the atmosphere, and can be used to measure the distance to, or other properties of a target by illuminating the target with light.

Differential Absorption LIDAR (DIAL) is a technique for monitoring of a particular gas in the atmosphere, such as carbon dioxide and water vapour [4]. DIALs are essentially dual – laser beams based upon different wavelength, one beam is absorbed by the gas of interest and the other is not absorbed. By taking the absorbent energy difference between the two beams, concentration of the gas can be evaluated as a function of range. DIAL technique relies on the unique absorption spectrum of each molecule. An absorption measurement is made with laser light, at a peak of absorption and at a trough, giving a differential signal. Using Tm^{3+} (thulium) and Tm^{3+} - Ho^{3+} (thulium-helium) doped solid-state lasers operating at ~ 2 μm in differential absorption lidar has been reported [5, 6]. Several researches of lasers operating around ~ 2 μm have been developed in the surgery field [7] as well as various other medical applications [8].

Among all rare earth elements, thulium (Tm^{3+}) as one of the best active ions is an obvious candidate for infrared domain applications. It is of interest because of its broad emission spectrum and its interesting emission in the 1.8 μm spectral region. In addition Tm^{3+} has advantage of absorption at 790 nm which is available using commercial diodes. Another important feature is the so called "Cross-relaxation" process in which for each pumping photon yields two ions in the upper laser level. This is benefit for 1.8 μm transition and providing pump quantum efficiency close to 200%. Because of Tm^{3+} emission at S-band which occurs for the $^3H_4 \rightarrow {}^3F_4$ transition, Tm^{3+} doped glasses and fiber amplifiers has significant attracted interest in 1.4 μm broadband application [9]. In Tm^{3+} system, lasing close to 2 μm wavelength area finds several possible applications making them an invaluable device. Lasers operating at around 2μm are easily and quickly absorbed by water, thus they have particular character in the medicine field, where they are used for the precise cut and ablation of biological tissues [10-12]. In addition 2 μm lasers are good choice for light detection and ranging application [13]. Various glasses including silica, fluoride, germinate have been used as laser host material. An alternative host material is tellurite glass. Amongst of all oxide glasses, tellurite have the lowest

phonon energies (~ 750 cm^{-1}), which lead to increase in optical efficiency and decrease in probability of non-radiative multiphonon decay. Another feature of tellurite glass is high rare earth ions solubility comparing with silicate and germinate hosts. In fact the concentration quenching effects in tellurite glasses is less than other hosts due to their multiplicity of structural units: TeO_4 bipyramid, TeO_3 pyramid, and polyhedron [14]. Moreover, tellurite glass as a heavy metal oxide glass combines good mechanical stability, chemical durability and a wide transmission window, which make them the best choice for photonic applications [15-19]. Through these properties, tellurite glasses are performed well at wavelength domain where other heavy metal oxide glasses do not. A number of literatures have reported on the implementation of tellurite glasses in optical devices systems [20-22]. Much attention has been considered to Tm^{3+} doped tellurute fibers and glasses, because of providing highly coherent light sources and multiple wavelength regions at 1.5 and 2 μm [23]. However laser development relies on accurate modelling and comparison of different glasses require being able to know the main spectroscopic quantities over a large interval of Tm^{3+} ion concentrations. Different Tm^{3+} concentrations samples from 0.36 up to 10 mol% have been studied to find an optimum Tm^{3+} concentration value and optical properties of Tm^{3+} doped glass samples were investigated under pumping at 785 nm.

In this study, cross relaxation parameters were calculated based on the extracted formulas from the rate-equation system. Two techniques were used for measuring the cross-relaxation parameter (C_R). In the first one the C_R was calculating by using data from the measurement of the experimental lifetime of the $^3H_4$ level. The second technique is investigation the steady state emission of radiation from both levels $^3H_4$ and $^3F_4$. These two approaches are discussed in chapter three. A simulation was carried out to see how cross relaxation parameter influences the emission intensities of $^3H_4$ and $^3F_4$ levels. An example of this simulation has been reported in the third chapter of this thesis. Fluorescence decay measurements were conducted as well to determine the lifetimes of the $^3H_4$ and $^3F_4$ manifolds as a function of the Tm^{3+} ions concentration.

In this spectroscopic investigation one of the important aspects is concerns of different concentration of Tm^{3+} doped tellurite glasses in order to identify the required thulium doping level to develop a compact Tm-doped tellurite fiber laser. To achieve this target, it is very important to understand the rare earth ion concentration, because of its impact on lifetime values and energy transfer mechanisms. The high concentration improves quantum efficiency, because of a good overlapping between emission spectrum of the sensitizer and absorption spectrum of the activator. However, reverse cross-relaxation mechanism occurs over a specific concentration level. To ensure robust single-frequency operation a compact cavity is needed and therefore to generate power in excess of few hundred of mW, high active ion concentration is needed.

Aims and Objectives

In this thesis, a spectroscopic investigation of Tm^{3+} highly doped tellurite glass has been carried out. Various features, optical properties and characteristics of thulium and tellurite are outlined in this work. Analysing of the equations system and the associated numerical modelling of three level laser system is another aspect of the aims. The objective of this thesis was spectroscopic investigation of thulium doped tellurite glass technique to improve the quantum efficiency of this laser system. The present investigation concerns of tellurite based host composition (TZN). The TZN host composition was doped with active ions in different concentrations. High doping concentration increases quantum efficiency due to good overlapping between sensitizer absorption and acceptor emission spectra. However, a concentration quenching processes take place over a certain concentration values.

Chapter II

Glass – Tellurite glasses

Introduction

Glass can be doped with rare earth ions which give it special photonic properties. Several advantages include excellent homogeneity, unique structural and thermodynamic features make glasses have great potential for photonics. The transition from a viscous liquid to a solid glass is called "glass transition" and the temperature corresponding to this transition is called "glass transition temperature" (Tg). Its transformation into crystal occurs if re-heated to a temperature above Tg, which in this case called "glass crystallization temperature" (Tx) [24]. For instances, there are several important glass systems including oxide glasses (silica, silicate, and non-silicate), halide and oxy-halide (fluoride, fluorophosphate) and cholcogenide. Glass components can be divided into three different types considering their function (network formers, modifiers, and intermediate) [25]. Formers can form a glass by itself, while modifiers incorporates into a glass host to restructure and modify the glass characteristics, such as the glass transition temperature [26, 27] and the nonlinear optical response [28]. The intermediate is possible in case amorphous network when added to the network former.

The silica glass has been widely used in the various optical devices [29]. An alternative type of host glasses are used for particular applications involved tellurite glasses. These glasses exhibit wide transmission region, high glass stability, high rare earth ion solubility, low cut off phonon energy of around 750 cm^{-1}, good resistance to corrosion, high refractive index [30]. The previous mentioned features make tellurite glasses become promising host for MIR lasers at 2.0 μm wavelength. Comparing to 880 and 1100 cm^{-1} in germinate and silica respectively, the low phonon energy feature of tellurite glass (750 cm^{-1}) allows transmission further into the IR.

2. 1. Features of tellurite glasses as a host material

As mentioned at the beginning of this chapter, the tellurite glasses are characterized by important features, which will be presenting in some details through the next subsections.

2.1.1 Low phonon energy

According to quantum theory, microscopic vibrations in solid media are quantized. Energy of vibration occurs in that media are referred as phonons. They influence the lifetime, i.e. they lead to very fast transitions between sublevels of manifolds of ion. As a result, fast thermalisation of levels and significant lifetime broadening takes place. In addition, phonons can cause multi-phonon transitions between the levels, which can reduce the laser efficiency in some cases. The transitions between manifolds can be radiative or nonradiative. In some cases quenching of radiative transitions takes place [31].

2.1.2 Refractive index

In general the refractive index parameter that determines the optical characteristics of the material is expressed as relation between speed of light in vacuum and speed of light in material concerned. The velocity of light in vacuum is greater than that in the medium. The measuring of the refractive index shows us how much the speed of light is reduced inside the medium. For example, tellurium oxide (TeO_2) based glass has a refractive index (1.95-2.05), which means that in this glass, the speed of transformation data can be $\cong 0.5$ the speed of light in vacuum. The high refractive index of TeO_2 results in high absorption and emission cross sections [32].

2.1.3 Solubility

The uniform dispersion of the rare earth dopant in glasses greatly alleviates the clustering problem and maintains the efficiency of the laser [33]. The solubility of tellurite glass was proved based on the absorption spectrum [34]. In comparison with silica, the literature [14,35] pointed out that rare earth ions have a high solubility in tellurite glasses [36].

2.1.4 Transmission range

Tellurite glasses based on TeO_2 have a wide optical transmission range from 0.35 to 5.5 μm. The wide transmission ranges of these glasses allow the observation of rare-earth doped lasers emissions in a large optical range. This feature, coupled with good resistance to corrosion and high mechanical stability, make tellurite glasses become promising host for mid-IR lasers at 2.0-μm wavelength [37, 38].

2.1.5 Thermal stability and corrosion resistance

Tellurite glass with network former TeO_2 has good glass formation ability. The thermal stability of Er^{3+} / Yb^{3+} co-doped tellurite glasses were investigated in several literatures [39]. Knowing the glass crystallization temperature (Tx) and the glass transition temperature (Tg) can help to define the glass thermal stability (ΔT) by the expression $\Delta T = Tx - Tg$. For fiber drawing ΔT should be large enough, i.e. $\Delta T \geq 100$ °C [40]. In comparison with silica in which Tg = 1100 °C, the glass transition temperature of the tellurite is about 300 °C and the crystallization temperature up to 470 °C [35].

2. 2. Structure of tellurite glass

To optimize the optical properties of rare earth ions in glasses, it is necessary to select suitable network modifier [41]. The existence of the modifier ions into any composition may provide a broad absorption and emission spectra [42]. Using modifiers in tellurite composition make it easy to formulation and improve their properties [43]. Tellurite glasses accept the following modifiers: alkali oxides (Na_2O, Li_2O, K_2O), earth alkali oxides (MgO, CaO, BaO), and zinc oxide (ZnO). The general formula of the tellurite composition in our study is (TeO_2, ZnO, Na_2O). Here TeO_2 is the glass former, which characterises by wide transmission region, good thermal stability, low phonon energy and high linear refractive index and nonlinear efficient.

Zinc oxide (ZnO) is more easily integrated inside the system than sodium, because the number of replaceable atoms is similar to that in tellurium oxide. The sodium oxide content (Na_2O) is the glass modifier. The latter can be used to change various properties of the material, such as the glass transition temperature [25].

2. 3. Luminescence properties of rare earth elements

2.3.1 The 4f electron shell

Rare earth ions are divided in two groups. The first one is lanthanides, which starting with element of atomic number 57 and ends with element of 71. The second group is actinides with atomic number 89 up to 103. As most of the isotopes of the actinides are unstable, the majority of fibers have been doped with lanthanides ions, which characterised by stable triply ionised form [44]. The first atomic structure calculations have been reported in [45] by M. Mayer, who theoretically explained the sharp absorption lines in the spectrum of rare earth. The trivalent state (3^+) is the most common form of lanthanide elements. These trivalent lanthanide ions have an electronic configuration identical to Xenon structure, to which a certain number (1-14) of 4f electrons have been added [46]. Therefore, the electronic states of these rare earth ions are determined by the electronic configuration of the $4f^N$ level. Shielding of 4f electrons by the 5S and 5p shells is responsible for $4f \rightarrow 4f$ optical transitions and all atomic properties of the lanthanides. In some literature lists of lanthanides ions with their atomic numbers and electronic configurations were reported [47].

2. 4. Ion - Ion Interactions

The interactions between active centres can be considered in two approaches. First one is microscopic interactions and the second is macroscopic. The former studies the theoretical interactions between centres. The latter related to the experimental conditions of the ions. Microscopic includes several processes, which are presented in the next sections.

2.4.1 Energy Transfer (ET)

The most important demonstration of interaction between rare earth ions is the energy transfer process. It may occur among different or same type of ions. Energy transfer can have a negative impact on the amplification. For example in the situation of depletion of the upper state in Er^{3+} doped tellurite glass. In some cases energy transfer can be used positively. For instance in the case of the infrared pumped visible lasers [48]. Energy transfer from an excited ion to a nearby ion in its ground state without gain or loss energy is known as resonant energy transfer. It is illustrated in Fig.2.1. This kind of ET is characterized by emission and absorption of photon between the donor (sensitizer) and acceptor (activator) ions. Probability of the resonant energy transfer can be expressed as [30],

$$P(R) = \frac{\sigma_a}{4\pi R^2} \cdot \frac{1}{\tau} \cdot \int g_1(v) g_2(v) dv \qquad (2.1)$$

Where σ_a is absorption cross section of an acceptor, τ is lifetime of the donor, $g_1(v)$ is line shape function of the sensitizer emission and $g_2(v)$ is line shape function of the activator absorption. The integral in equation 2.1 explains that excitation can be transferred between donor and acceptor ions only if there is energy overlap between them. R represents the distance between two ions. Probability P(R) of the ET describes photon trapping as well. This phenomena was investigated in literature [49].

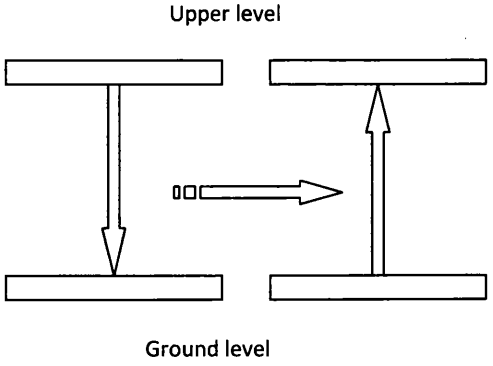

Fig.2.1 Resonant energy transfer

Non-resonant transfer takes place where the different energy between both levels is made up with assistance of a phonon. In addition, energy transfer can occur between ions in their excited states as in up-conversion process. To improve the efficiency of laser and amplification, good understanding of energy transfer processes between ions is required. Dexter was the first who developed the theory of energy transfer in solid material. He reported that there are two factors to improve the probability of energy transfer. The first factor is the average ion-ion distance, and the second one is the matched energy levels of ions [50].

2.4.2 Cross relaxation (CR)

Cross relaxation is a process of energy transfer in which an excited ion transfers part of its excitation energy to a neighbouring ion in the ground level. Therefore, the adaptor and the acceptor end up in some intermediate level. In cross relaxation energy transfer process, the optically excited ion is referred to as the 'donor' ion, whilst the ion accepting the energy is known as 'acceptor' ion. Cross relaxation as ion-ion energy transfer requires only that both donor and acceptor ions have two manifolds of identical energy gap. The probability of the CR can be calculate by using Judd-Ofelt parameters, integral of the donor – acceptor overlapping and dipole-dipole ET assumption [51]. Cross-relaxation process can be helpful and can be involved a single type of rare earth ion, which plays a role of donor and acceptor. The cross relaxation process can be used to increase the quantum and slope efficiencies of the lasing transition. The Fig. 2.2 illustrates the cross relaxation in thulium doped material.

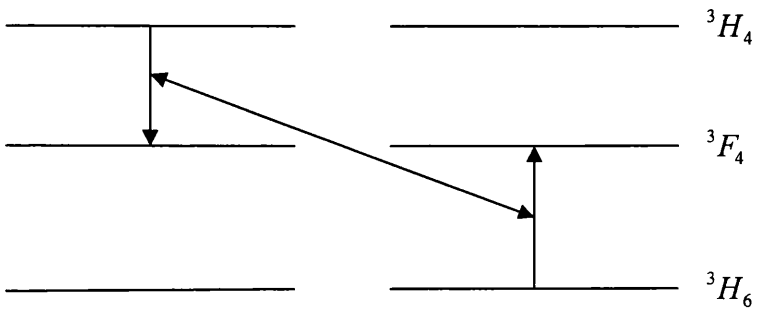

Fig. 2.2 Cross relaxation process between one ion in the exited state and another ion in the ground state

2.4.3 Up- conversion

One of the several types of energy transfer processes, which occur between ions, is up-conversion process. At high rare earth ions concentrations up-conversion phenomena occurs, which induce concentration quenching [52]. This leads to lower amplification efficiency. For instance in the case of the increasing concentration in erbium Er^{3+} content, the distance between neighbouring ions decreases and non-radiative energy transfer can occur ($^4I_{13/2}+{}^4I_{13/2}\rightarrow{}^4I_{15/2}+{}^4I_{9/2}$) as illustrates in Fig. 2.3. The donor ion in the $^4I_{13/2}$ level transfers its energy to neighbouring one at the same level. As the difference energy between $^4I_{13/2}$ and $^4I_{9/2}$ is close to that between $^4I_{13/2}$ and $^4I_{15/2}$, the donor falls to the ground state while the acceptor ion prompts to the higher level $^4I_{9/2}$.

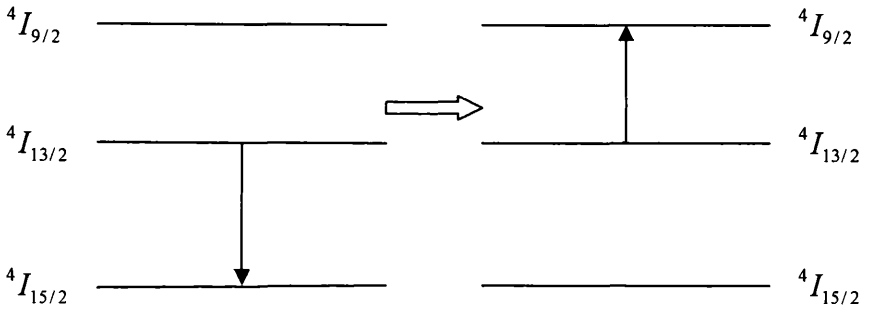

Fig.2.3 Up-conversion energy transfer between two neighbouring Er^{3+} ions located at the same level

2.4.4 Multi-phonon relaxation (MP)

Multiphonon relaxation processes between energy levels can occur by the simultaneous emission of several phonons. These processes arise from the interactions between the electronic levels of the rare earth ions and electric field resulting from the oscillating particles of the host lattice. It is important to understand the multiphonon process as its nonradiative relaxation influences the radiative quantum efficiency of the transition between the levels of rear earth ions. Fig. 2.4 illustrates the multiphonon relaxation process. When the energy gap between the

excited level and the next lower level is larger than the phonon energy, several lattices are emitted in order to bridge the energy gap. For energy conservation, the following condition should be satisfied:

$$N \hbar\omega = \Delta E \qquad (2.2)$$

Where ΔE – the energy gap between two energy levels, N – number of phonons, and $\hbar\omega$ – phonon energy. The multiphonon rates (W_{mp}) correlates with the energy gap (ΔE) by:

$$W_{mp} = Wo \exp [-\alpha \Delta E] \qquad (2.3)$$

Where Wo is the transition probability and α is expressed by

$$\alpha = (\hbar\omega)^{-1} \ln [N/g(n + 1)]^{-1} \qquad (2.4)$$

where g is the electron phonon coupling constant and n is occupation number. The equation 2.3 is only approximate because both α and W_{mp} depend on ΔE.

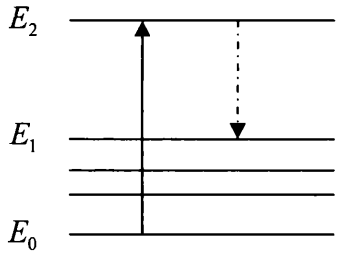

Fig. 2.4 Multi-phonon relaxation

2.4.5 Macroscopic approach

The value of the energy transfer between ions depends on spectral overlap between sensitizer emission, and activator absorption, mutual ion distance, and quantum transition efficiency [53]. In fact, the donor-acceptor interaction will depend on their concentrations, i.e. depend on the mutual distance between the donor and acceptor. In glass material systems three different interaction processes can be observed between the centres, which affect the form of the fluorescence decay: (1) direct energy transfer (2) diffusion-limited relaxation and (3) fast diffusion [54].

1. *Direct energy transfer*

This case of the interaction processes can demonstrate when a sensitizer ion transfers its energy to an activator ion. Let's consider ϕ ($\vec{r}$, t) the probability that the donor ion is in the excited state at position $\vec{r}$ at time't'. In the condition of the absence of activator and energy diffusion within sensitizers, the sensitizer ion system ϕ (t) will decay as a single exponential in form e^{-t/τ_0} where τ_0^{-1} is the intrinsic sensitizer decay rate. The sensitizer and the activator ions can exchange their energies by direct multi-polar transfer if their sites are inside the critical region. The general solution for the fluorescence decay ϕ (t), for multi-polar coupling is given by Inokuti-Hirayama equation [21]:

$$\phi(t) = \phi(t = 0)\exp\left(-\frac{t}{\tau_0} - \frac{4}{3}\pi \cdot \Gamma\left(1 - \frac{3}{S}\right) \cdot C_a \cdot R_0^3 \cdot \left(\frac{t}{\tau_0}\right)^{3/S}\right) \qquad (2.5)$$

Where $\phi(t = 0)$ is the initial excitation, R_0 is the critical transfer distance and C_a is the concentration of acceptor ion, S is the multi-polar parameter (S = 6, 8, or 10 for dipole-dipole coupling, dipole-quadruple, or quadruple-quadruple respectively).

2. *Diffusion-limited relaxation*

The diffusion-limited relaxation occurs when the rate of the energy diffusion within the donor system to acceptors is slow but still comparable to the intrinsic decay rate [21]. A general solution for case of diffusion-limited relaxation within the sensitizer system and sensitizer- activator energy transfer via dipole-dipole interaction was obtained [55].

3. *Fast diffusion*

This form of ET occurs in the systems with high sensitizer ions concentration. The fast diffusion ET exists between sensitizer ions by transfer the energy from one sensitizer to another until the excitation comes into the vicinity of activator ion, where sensitizer-activator ET can take place. The distances between sensitizer ions are small, as the concentration of ions is high. This lead to rapidly diffusion and the fluorescence decay of sensitizer will be exponentially dependence with time

$$\phi(t) = \phi(0)\, e^{-\left(\frac{1}{\tau_O}+\frac{1}{\tau_D}\right)t} \qquad (2.6)$$

Where $1/\tau_D = UN_A$, and 'U' depends on type of the interaction. The formula (2.6) says that donor rate is proportional to acceptor concentration [56]. Energy transfer rate (K) in high sensitizer concentration case can express as

$$K = 1/\tau_{SA} - 1/\tau_S = N_A W \qquad (2.7)$$

where W is independent on the concentration. The τ_{SA} and τ_S are the lifetimes of the sensitizer-activator and sensitizer alone respectively.

The direct transfer and the diffusion-limited relaxation as theoretical frameworks were reported in many literature to describe the non-exponential decay of the rare earth elements. Non-exponential decay of the $^3H_4$ and $^3F_4$ levels of thulium doped host materials explaining these two ET types were pointed out [57-59].

2. 5. Characteristics of the thulium and ytterbium

Thulium and ytterbium as active ions play an important role in the investigated luminescence processes. Doping with rare earth elements will form active glasses, which can be used into the laser and amplifier applications. In this research work, the main attention is devoted to the thulium (Tm^{3+}) as the main emitter. Many possible transitions and decays can occur in Tm^{3+} doped glass system and it is beneficial to give an overview of all possible ET mechanisms that occur in RE doped glasses.

2.5.1 Thulium (Tm^{3+}) spectroscopy

In recent years, there has been a significant interest to investigate Tm^{3+} doped material, because of its attractive emissions in the visible and infrared regions [60, 61]. Thulium doped glass appeared a broad wavelength band from 1600 to over 2000 nm. This wide band considerably attracts attention for tuneable lasing in the 'eye

safe' wavelength domain [1]. Literature pointed out another possibility of tuning in the 2200-2460 nm region in Tm:YLF [1]. The favourable spectroscopic characteristics of thulium, particularly absorption at 790 nm and its interesting emission at 1.8 nm make them as a good choice for infrared region applications include medical and biosensor [55]. Moreover, the self-quenching process (cross relaxation) $^3H_4$, $^3H_6 \rightarrow {}^3F_4$, $^3F_4$ produces two ions by one pump at higher laser level $^3F_4$, which intensifies the 1.8 μm emission. A significant effect of this process in the case of high dopant concentration and high pumping power can occurs. The transitions between levels during CR process deemed to be as a phonon assisted, which is exponentially dependence on the energy difference between $^3H_4 \rightarrow {}^3F_4$ and $^3F_4 \rightarrow {}^3H_6$ gaps. The exponential formula, which explains the dependence relationship of energy difference between the transitions has been reported by Miyakawa – Dexter [62]. Fig. 2.5 shows the cross relaxation mechanism in Tm^{3+} ion.

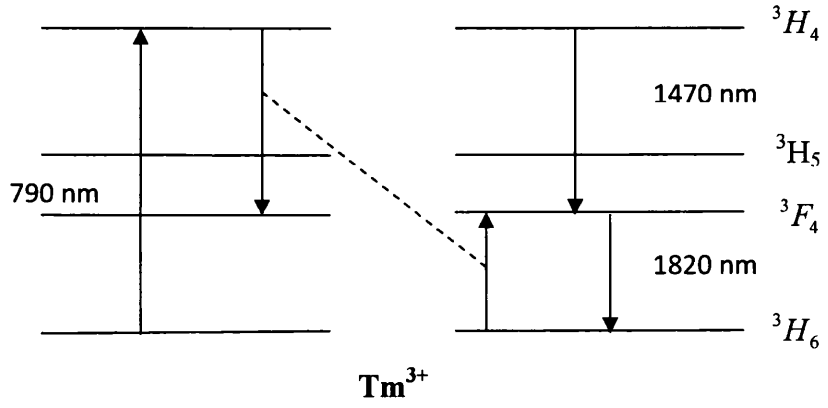

Fig. 2.5 Cross-relaxation mechanism in Tm^{3+}

In addition, an important emission is at 1.47 μm which occurs for $^3H_4 \rightarrow {}^3F_4$ transition. The lifetime of the $^3H_4$ level is shorter than that of the $^3F_4$ level. A diversity of pumping schemes of Tm^{3+} systems at wavelengths ~790 nm, ~1200 nm and ~1600 nm have been used in literature [63, 64]. With pumping at 790 nm, Tm^{3+} ions are excited to the $^3H_4$ energy level and an excited state absorption (ESA) may occur as well. Thus, Tm^{3+} ions from $^3H_5$ level may prompt to $^1G_4$ level as shown in Fig. 2.6. Two visible emissions, the blue one is at 478 μm ($^1G_4 \rightarrow {}^3H_6$) and the red transition is at 650 nm ($^1G_4 \rightarrow {}^3H_5$) were considered. Since $^3F_{2,3}$ and $^3H_5$ levels are

very close to the $^3H_4$ and $^3F_4$ respectively, then transitions $^3F_{2,3} \rightarrow {}^3H_4$ and $^3H_5 \rightarrow {}^3F_4$ are characterized non-radiative.

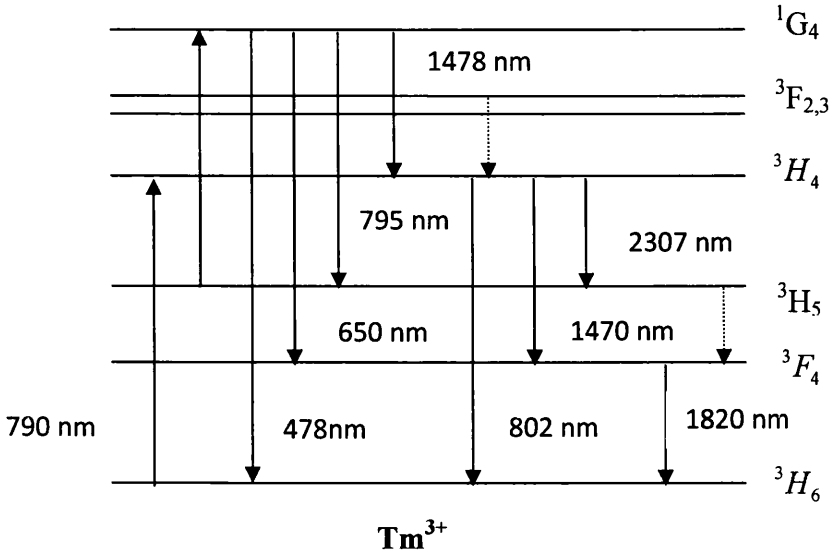

Fig. 2.6 Correspondent emission wavelengths for Tm^{3+}

At low dopant concentrations the energy transfer does not occur, however at highly $Tm3^+$ concentration energy transfer process will increase until a certain value, at which reverse cross relaxation starts up. Clustering can be occurs at high concentrations as well, leading to quenching concentration [62]. In some cases the acceptor ion is not in their ground state level, therefore the up-conversion energy transfer (ETU) and excited state absorption (ESA) processes are introduced. In the former process, one of the two excited $Tm3^+$ ions from the $^3F_4$ ends at $^3H_6$ level while the second ion transfers up to a higher energy level. Fig. 2.7 shows this process in Tm^{3+}. Existing ETU process in Tm^{3+} leads to depopulate $^3F_4$ energy level, which has a negative effect on emission from this level and laser performance [65]. ESA process is the same of the ETU, in which excited ion into $^3F_4$ level absorbs another photon and prompts to higher energy level. In such process, two photons are needed as shown in Fig. 2.7. The ESA process enhances emission from $^3H_4$ level.

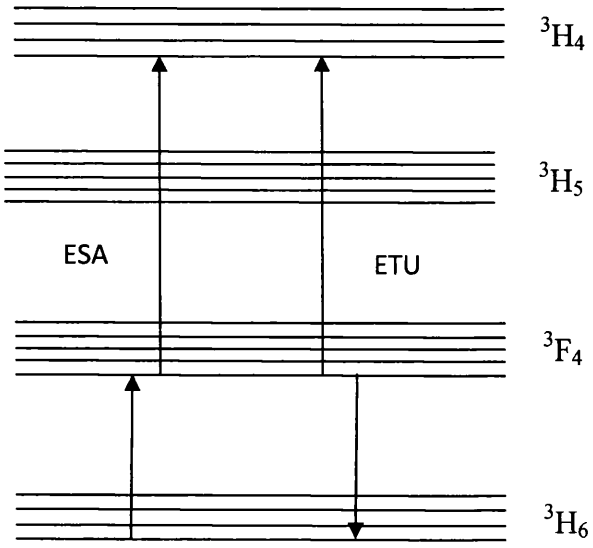

Fig. 2.7 Excited state absorption and up-conversion energy transfer in Tm^{3+} system.

Re-absorption or self-trapping is a resonant process which can considered as a result of interaction between two thulium active ions. The effect of this process it can be remarked in Tm^{3+} at $^3F_4 \rightarrow {}^3H_6$ transition [66].

.

2.5.2 Ytterbium (Yb^{3+}) spectroscopy

Ytterbium ions have a number of important characteristics which make them of practical interest. The Yb^{3+} energy levels system consisting of two manifolds. The ground state level $^2F_{7/2}$ and the excited-state level $^2F_{5/2}$. It has only one absorption band at 977 nm due to $^2F_{7/2} \rightarrow {}^2F_{5/2}$ transition. Yb^{3+} as a laser-active ion has very attractive emission characteristics involved long lifetime which is quite beneficial for storing energy, broad emission lines and simple electronic structure, which prevents parasitic de-excitation by cross-relaxation (CR), up-conversion energy transfer (ETU) or excited state absorption (ESA) [67, 68]. In addition, low heat capacity, high energy conversion efficiency and high quality laser beam are available due to no concentration quenching. ESA, up-conversion and multi-phonon relaxation occur in this ion [69]. Because of the wide energy gap between the Yb^{3+} manifolds (~ 10500 cm^{-1}), non-radiative multi-phonon decay is prevented and the relaxation from the

excited state $^2F_{5/2}$ is radiative in the majority of host materials [70, 71]. In addition ytterbium doped glass has a broad absorption and emission spectrum that enable them for tuneable laser [31]. The above features contribute to the high efficiency of operation that can achieve in ytterbium lasers. Furthermore, Yb^{3+} has been widely used as a sensitizer for Er^{3+} [72], Tm^{3+} [73], Pr^{3+} [74], and Ho^{3+} [75], because of its an intense broad absorption cross section.

2.5.3 Yb^{3+} / Tm^{3+} spectroscopy

Employing the $Yb3^{+}$ / Tm^{3+} ions system can convert the wavelength pump to the short wavelength via multi-photon excitation process. Two types of excitation can be used to produce pumping of the upper laser level: direct and indirect. In our case, it is possible to achieve pumping of Tm^{3+} by Yb^{3+} energy transfer (indirect method). The $^2F_{5/2}$ level is located closer to the Tm^{3+} upper laser level than the initial level. This makes the energy transfer process much easier from intermediate to the upper one than pumping directly from initial level. The possible up-conversion mechanisms for the blue and red emissions based on the Tm^{3+} / Yb^{3+} system are presented in Fig. 2.8.

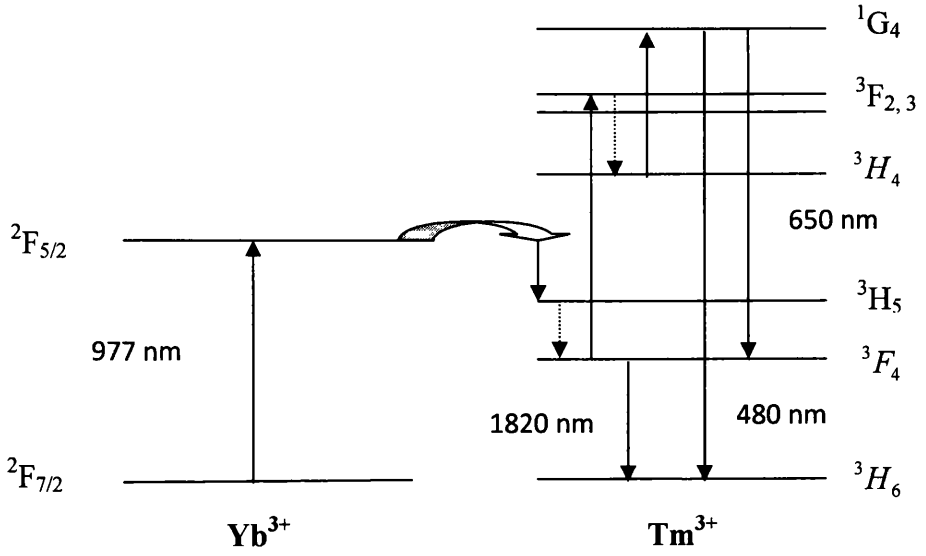

Fig. 2.8 Up-conversion mechanisms for Tm^{3+} / Yb^{3+} system. Dashed arrows denote non-radiative process

The upper level $^2F_{5/2}$ of the Yb^{3+} ion can be excited by 977 nm source. Both transitions (red and blue emission) can be explained as follows: As a result of the absorption ground state level of Yb^{3+} ion, consecutive excitation processes occur in Tm3+. Non-radiative energy transfer from Yb^{3+} ion excites the Tm^{3+} in the $^3H_5$ level. Energy from $^3H_5$ can be transferred to $^3F_4$, $^3F_{2,3}$ and $^1G_4$: $^2F_{5/2} + {}^3H_6 \rightarrow {}^2F_{7/2} + {}^3H_5$. Tm^{3+} in the $^3F_4$ level is excited to $^3F_{2,3}$ level by both ET: $^2F_{5/2} + {}^3F_4 \rightarrow {}^2F_{7/2} + {}^3F_{2,3}$ and ESA: $^3F_4$ + photon$\rightarrow {}^3F_{2,3}$. Another excitation occurs from the $^3F_4$ level to the $^1G_4$ level by nonradiative ET from Yb^{3+} and ESA: $^2F_{5/2} + {}^3F_4 \rightarrow {}^2F_{7/2} + {}^1G_4$ and $^3H_4$ + photon$\rightarrow {}^1G_4$ [76]. Several radiative decay processes can occur involved: $^1G_4 \rightarrow {}^3H_6$ at 480 nm (blue emission), $^1G_4 \rightarrow {}^3F_4$ at 650 nm (red emission) and $^3F_4 \rightarrow {}^3H_6$ at 1.8 μm.

The higher Yb^{3+} ion concentration, the shorter distance between Tm^{3+} and Yb^{3+}, this lead to possibility of back transfer process ($^3F_4$, $^2F_{7/2} \rightarrow {}^3H_6$, $^2F_{5/2}$), which related to the lifetime by [77]

$$K = \frac{1}{\tau(3_{H_4})_{Yb-Tm}} - \frac{1}{\tau(3_{H_4})_{Tm}} \qquad (2.8)$$

Where $\tau(^3H_4)_{Yb\text{-}Tm}$ and $\tau(^3H_4)_{Tm}$ are the lifetimes for the co-doped and singly doped samples, respectively.

2. 6. Three and four level lasers

According to pumping scheme, lasers are classified as two, three, or four-level systems. Although the energy level schemes of the ions are very complex, they can be simplified and considered only as N-fold system. The symbol N here represents the number of levels in the excitation and lasing. A schematic of the three-level system [78] is shown in Fig. 2.9.

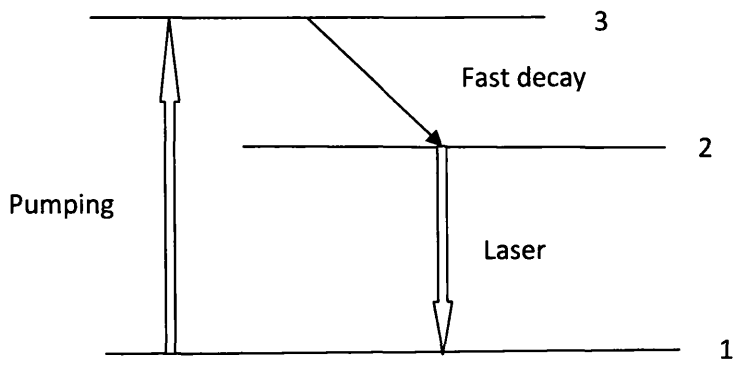

Fig. 2.9 Three level system

Initially, all atoms of the laser materials are at ground level 1. The pump light raises these atoms from the ground level into the excited level 3. This process is called pumping. Most of the excited atoms decay rapidly and non-raditively into the intermediate level 2. Finally, the atoms return to the ground level by the emission of a photon. The last transition is responsible for the laser action.

Population inversion can be obtained by studying their conditions with three level system in Fig. 2.10. Then the population inversion can be defined by formula [46]

$$\Delta N = N_2 - N_1 = \frac{w_p - A_{21}N}{w_p + A_{21} + 2w_{12}^{ST}} \qquad (2.9)$$

Where w_p is the rate of pumping between levels 1 and 3 ($w_p = w_{13}$), N is the total ion number density, and A_{ij} is the inverse of the radiative lifetime.

For net amplification $\Delta N > 0$, implies $w_p > A_{21}N$ – the pump rate must exceed the decay rate by spontaneous emission.

.

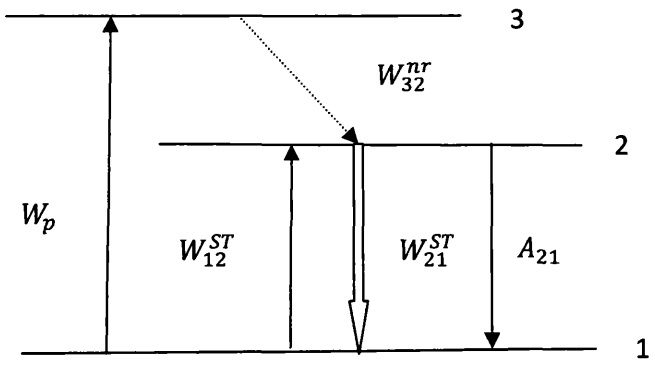

Fig. 2.10 Transitions involved in optically pumped three- level system

Stimulated absorption at the signal wavelength W_{12}^{ST} may occur in three- level system. The W_{12}^{ST} process reduces the pump efficiency, which is reducing the gain of the laser. In four-level pumping scheme this does not occur. Fig. 2.11 shows the four-level system [78].

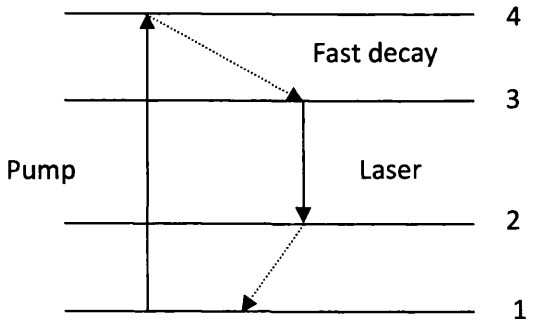

Fig.2.11 Four-level system

The population inversion in four-level system can be calculated by formula [46]

$$\Delta N = N_3 - N_2 = \frac{w_p \tau_{rad}}{1 + w_p \tau_{rad}} N \qquad (2.10)$$

Where w_p is the rate of pumping between levels 1 and 4 ($w_p = w_{14}$).

Amplification due to the $^3H_4 \rightarrow {}^3F_4$ transition at 1.47 μm of Tm^{3+} is classified as four-level system amplification. Lasing due to $^3F_4 \rightarrow {}^3H_6$ transition at 1.8 μm of Tm^{3+} is classified as three-level system. In the four-level system the lower level of lasing is the intermediate state, while in the three-level is the ground state, which can be considered as a serious disadvantage.

2. 7. Excited state lifetime measurements

Lifetime measurements can be conducted via exposing the media of laser to an excitation beam. The interaction between the beam and media causes fluorescence emission. Its character, which describes several physical processes, can be measured under particular procedures. Lifetime is defined as the time in which the emission intensity falls of the factor of 1/e of maximum. To calculate lifetime three methods are possible: a) Exponential fit. b) Power exponential fit. c) Average lifetime calculation.

1. ***Exponential fit***

Lifetime value in exponential decay situation can be calculated using the following formula:

$$I(t) = I(t_0)\, e^{-t/\tau} \qquad (2.11)$$

2. ***Power exponential fit***

This method shows the assumption of deviation from exponential fit by using the power factor in the exponential fit. The method can be used to compare the shapes and decay time scales between different systems. It expressed by the next form:

$$I(t) = I(t_0)\, e^{-(t/\tau)p} \qquad (2.12)$$

According to the equation (2.12), there are three parameters which describe the decay function. $I(t_0)$ parameter is the initial population of the excited level, τ is the lifetime of the excited level, and P is the exponential power.

3. Average lifetime

This approach is used in the cases where the waveform decay is non-exponential. Lifetime value in this situation can determine by formula [79]

$$\tau = \frac{1}{I(t_0)} \int I(t)dt \qquad (2.13)$$

2. 8. Concentration quenching

2.8.1 Self quenching

The general picture of self quenching is that arising of the ion concentration leads to an increasing in the diffusion in the form of non-radiative transitions [80]. The fluorescence can be lost by static quenching or inner filter effect. The self-quenching is a special case of static quenching, in which the fluorophore and quencher are the same species. Inner filter effect is a measurement artefact instead of quenching process. It occurs in samples with very high absorbance. The self-quenching behaviour for the limited diffusion case can be described by a quenching rate R_Q:

$$R_Q = \frac{1}{\tau} - \frac{1}{\tau_m} = KN^2 \qquad (2.14)$$

Where τ is the measured lifetime at given concentration N and τ_m is the lifetime for low concentration (radiative lifetime). In direct way Weber [54] has expressed the constant K in the case of sensitizers diffusion and dipole-dipole interaction as: $K = 8\pi C_{SA}^{1/4} C_{SS}^{3/4}$, where C_{SA} is the transfer constant between sensitizer and activator and C_{SS} is the transfer constant within sensitizers. Dexter has presented the C_{SA} and C_{SS} in one formula [81]: $C = (R_0 / R)^S/\tau_S$. R_0 is the critical distance between sensitizer and trap, R is the distance between the two interacting ions, S is the multi-polar index and τ_S is the sensitizer lifetime. Similarly, Weber constant (K) is given in form $K = \frac{9}{2\pi\tau_m N_0^2}$, in which N_0 is a critical sensitizer concentration defined in terms

of a range parameter R_0, where $N_0 = \frac{1}{\frac{4}{3}\pi R_0^3}$ [81]. By manipulating the K and R_0 parameters the following formula can be obtained:

$$\tau = \tau_m/[1 + \left(\frac{9}{2\pi}\right)\left(\frac{N}{N_0}\right)^2] \qquad (2.15)$$

By equation (2.15), measured lifetime values can be fitted for identifying the τ_m and N_0 values[80].

2. 9. Non-radiative rate

One of the microscopic mechanisms that contribute to characterization of any laser dynamic is non-radiative decay from excited to lower energy level. Good understanding of lanthanide luminescence required clearly evaluation of the non-radiative contribution. The total decay rate (W_T) from an excited state level is defined as:

$$W_T = Wr + W_{nr} \qquad (2.16)$$

Where W_r is the radiative transitions rate and W_{nr} is the nonradiative transitions rate. The W_{nr} term involves multi-phonon relaxation rate (W_{mp}), energy transfer rate (W_{ET}), and hydroxyl 'OH' groups rate (W_{OH}), which illustrates the energy transfer rate between active ions and hydroxyl groups [79]. Therefore the nonradiative decay rate is given by

$$W_{nr} = W_{mp} + W_{ET} + W_{OH} \qquad (2.17)$$

The multi-phonon decay rate occurs due to phonon or impurity vibrations when an ion decays to lower level by emission or absorption process. W_{mp} can be defined by Miyakawa – Dexter formula [82, 83]:

$$W_{mp} = C.[1 + \frac{1}{\exp\left(\frac{\hbar\omega}{KT}\right)-1}]^{\Delta E/\hbar\omega}.e^{-\Delta E.\alpha} \qquad (2.18)$$

Where C is the host-dependent parameter, ΔE is the energy gap of the transition, $\hbar\omega$ is the phonon energy, K is the Boltzmann constant and T is the temperature of the material. The coupling parameter 'α' is given by $\alpha = \frac{1}{\hbar\omega}\ln\left[\frac{N_i}{g_s(n+1)}\right]^{-1}$, where N_i is

the number of phonon, g_s is the electron-phonon coupling efficiency of sensitizer ion and n is the Bose-Einstein distribution of phonon occupation number. The Bose-Einstein distribution is expressed as n = 1/exp ($\hbar\omega$ / KT)-1.

2. 10. Quantum efficiency

The relation that describe the ratio between radiative rate (W_r) to the total decay rate which includes nonradiative and radiative part ($W_r + W_{nr}$) known as quantum efficiency (η). This relation can be expressed as ratio between measured and radiative lifetimes. In general this is ratio less than one, however in some cases it may take value more than one. The quantum efficiency formula can represents as following [84]:

$$\eta = \frac{W_r}{W_r + W_{nr}} = \frac{\tau_{meas}}{\tau_{rad}} \leq 1 \qquad (2.19)$$

From equation (2.19), it can be seen that the ratio between measured and radiative lifetime also presents the quantum efficiency. In the case of co-doped glasses, ET efficiency (η) can be calculated by measuring sensitizer lifetime (τ_S) and sensitizer-activator lifetime (τ_{SA}) [85,86]:

$$\eta = 1 - \frac{\tau_{SA}}{\tau_S} \qquad (2.20)$$

2. 11. OH Quenching

The presence of OH groups into RE doped glasses can seriously affect the fluorescence quantum efficiency of the emitting trivalent RE. OH groups may exist as a result of the starting materials and atmospheric moisture during the melt process [87]. To avoid the contamination of these groups, there are many procedures via variations in composition and synthesis. For example dry-air bubbling was done during the melt for decreasing the OH groups in glasses [88]. In addition it has reported that very low OH content were obtained in sodium alumino-phosphate glasses co-doped with Yb^{3+} and Tm^{3+} prepared in air [89].

2. 12. Radiative Transitions Theories

The following subsections describe several methods that can be used to calculate the radiative transitions or model their parameters.

2.12.1 Fuchtbauer – Landenburg Theory

The Fuchtbauer – Landenurg (FL) theory analyses the fluorescence spectrum. The FL equation is part of a procedure for defining emission cross section. According to this theory, the wavelength-dependent fluorescence intensity is proportional to the emission cross section times the fifth power of the optical frequency [90].

The relation between radiative lifetime and emission cross section can quantitively be described by the formula [57]:

$$\frac{1}{\tau_{rad}} = \frac{8\pi n^2}{c^2}\int v^2\,\sigma_{em}(v)dv = 8\pi n^2 \int \frac{\sigma_{em}(\lambda)}{\lambda^4}d\lambda \qquad (2.21)$$

Several forms are available of FL equations and with the assumption that the fluorescence intensity I (λ) is proportional to the emission cross section, FL equation takes form:

$$\sigma_{em}(\lambda) = \frac{\bar{\lambda}^4}{8\pi c n^2 \tau_{rad}} \frac{I(\lambda)}{\int I(\lambda)d\lambda} \qquad (2.22)$$

Where $\bar{\lambda}$ is the peak emission wavelength, n is the refractive index, C is the vacuum velocity of light, and $\frac{1}{\tau}$ =A is the spontaneous emission. The Fuchtbauer – Landenurg theory has been commonly used for rare earth elements and is grounded in the fundamental of the Einstein A and B coefficients.

2.12.2 McCumber's Theory

The absorption and emission cross-section parameters are used to explain the efficiency of the electromagnetic –ions interaction [91]. Thus, the absorption and emission spectra of the RE are the fingerprints of the energy levels of the 4f inner electrons [92]. Knowing the absorption and emission cross-sections, one can engineer the host material for active laser devices. In addition, by using the

absorption and emission cross-sections, the gain parameter of an optical medium can be calculated. The equation (2.23) shows how to calculate the gain through absorption and emission cross-sections [59]:

$$\gamma(\lambda) = N_2\sigma_{em}(\lambda) - N_1\sigma_{abs}(\lambda) = N_1[\frac{N_2}{N_1}\sigma_{em}(\lambda) - \sigma_{abs}(\lambda)] \qquad (2.23)$$

Where $\gamma(\lambda)$ is the gain of the medium (cm^{-1}), σ_{em} is the emission cross section, σ_{abs} is the absorption cross section and N_1 and N_2 are the population of the levels 1 and 2 respectively. As demonstrated by Mc Cumber [93], the emission and absorption cross sections are related each other as a following:

$$\sigma_{em}(\lambda) = \sigma_{abs}(\lambda).\exp[\frac{\varepsilon - h\nu}{KT}] \qquad (2.24)$$

Where h is the Planks constant, ν is the frequency of the wave emitted or absorbed, K is the Boltzmann constant, T is the temperature in Kelvin and ε is temperature dependent excitation energy.

The experimental emission cross section can be evaluated by:

$$\frac{1}{\tau_e} = 8\pi n^2 c.\int \frac{\sigma_e(\lambda)}{\lambda^4} d\lambda \qquad (2.25)$$

Where τ_e is the spontaneous emission lifetime and n is the host refractive index. The Mc Cumber theory is valid under certain assumptions for obtaining reasonable cross section values [94] including :

- The lifetime of the manifold is longer than that of the time taken to achieve thermal equilibrium in each manifold.

- The spectral width of every level is small when compared to thermal distribution KT.

This theory applied to explore the quantitative relations between different optical properties of laser gain media such as rare earth doped gain media. The Mc Cumber theory refers to the effective cross sections of absorption and emission of light in the physics of solid state lasers. The emission and absorption cross section are not

independent, they are related with each other as shown in equation 2.24. Mc Cumber theory does not allow determining the other important parameters such as radiative lifetime and branching ratios. Then another theory to evaluate these parameters will be presented in the next sub-section.

2.12.3 The Judd - Ofelt Theory

The Judd-Ofelt theory is powerful and important. It is widely employed to estimate transition probabilities between states of 4f system. In addition it used to look for new laser transition and to calculate radiative lifetimes and emission branching ratios. In case of studying the performance of doped glasses, it is important to have knowledge of the intensities of 4f states transitions. These spectral intensities can be obtained utilizing the JO theory [95, 96]. This theory can be used to analyze the absorption and emission spectra of rare earth ions in solids, and compute their transition properties, line strengths, energy lifetimes, and emission cross sections. The Judd-Ofelt parameters can be calculated with fluorescence lifetimes.

The ***spontaneous emission rate*** is given by:

$$A_{\acute{J}J} = \frac{64\pi^4 e^2}{3h(2J+1)\bar{\lambda}^3}\left[\frac{n(n^2+2)^2}{9}S_{ED} + n^2 S_{MD}\right] \qquad (2.26)$$

Where $\acute{J}$ is the total angular moment of the final state, S_{ED} is electric dipole line strength and S_{MD} is the magnetic dipole line strength.

The ***radiative lifetime*** can be expressed in terms of spontaneous emission probabilities as:

$$\tau_0^{-1} = \sum_J A_{\acute{J}J} \qquad (2.27)$$

The ***fluorescence – branching ratio*** from final state is given by:

$$\beta_{\acute{J}J} = \frac{A_{\acute{J}J}}{\sum_J A_{\acute{J}J}} \qquad (2.28)$$

Chapter 3

Modelling

3.1 Introduction

The modelling of a laser requires several input parameters to describe all processes. Then a set of parameters is usually needed to account for any laser system. For modelling systems, the challenge is in accurately measuring or predicting many of these parameters. The approach is then to make some assumptions regarding the energy transfer, transitions, and decay processes into the laser system.

Thulium doped laser systems are important sources for lasing close to 2 μm. This wavelength domain is attractive in a number of applications, such as medicine and surgery field and remote sensing applications. The 2 μm lasing sources have gained special interest, because of their potential for efficient pumped operation. However, lasers with these materials face key issues, including re-absorption, increased threshold and up-conversion processes. To develop efficient laser with thulium systems, it is benefit to study laser simulation models where the reported problems are taken into account.

3.2 Choice of pump wavelength

The absorption spectrum of thulium doped tellurite glass exposes various choices for a pump wavelength for thulium laser system. The most interesting pump wavelengths are at 800 nm ($^3H_4$ level), 1200 nm ($^3H_5$ level), and 1600 nm ($^3F_4$). Thulium has a strong absorption band near 800 nm, which correspond to the transition $^3H_6 \rightarrow {}^3H_4$. For this reason, a laser diode operating around 800 nm was used as the pump source.

Pumping Tm^{3+} system at wavelength 1600 nm makes it acts as two-level system. An in-band pumping scheme ($^3H_6 \rightarrow {}^3F_4$) was applied for 2 μm Tm^{3+} doped tellurite fiber laser [97]. The other possibility for pumping Tm^{3+} ions is pumping into the 1.2

μm, which correspond to the transition $^3H_6 \rightarrow {}^3H_5$ absorption band. However, in case of high-power, laser diodes emitting at this wavelength are not available. [98].

According to the above discussion, therefore, the 800 nm absorption band was chosen as a pump wavelength in our study. When Tm^{3+} doped glass pumped around 800 nm, emission undergoes in two broad bands. The first is centred at 1.4 μm, which is important in the development of fiber optic amplifiers. The second is centred at 1.8 μm which is also important for the construction of laser systems.

3.3 Modelling Tm doped glass

Lasing close to ~2 μm using tellurite glass host has been reported in literature [99]. Previously mentioned properties of tellurite glass make them an efficient and reliable host material. In this section, a proposed model has been used for studying some transitions in Tm^{3+} system. This model constituted on rate equations system, which describes the populations in the many energy levels. Behaviour of the laser system has been simulated. The rate equations were determined according to the energy level scheme of thulium, which shown in Fig. 3.1.

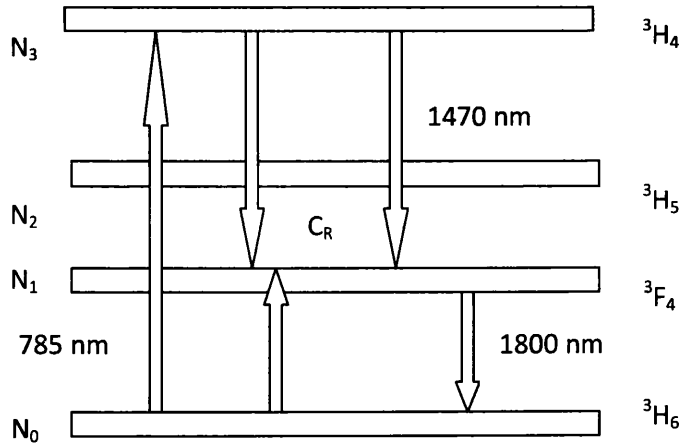

Figure 3.1 Simplified energy level diagram of Tm^{3+}

In Tm^{3+} diagram, the upward arrow from $^3H_6$ to $^3H_4$ level describes the pump power transition rate (W_{03}). The slide downward arrows from $^3H_4$ to $^3F_4$ (1470 nm) and $^3F_4$ to $^3H_6$ (1800) represent the signals of the radiative spontaneous emission. The arrows

C_R represent the cross – relaxation transition. The model of Tm^{3+} laser including the rate equations that describe the relationships between the pump and all transitions and processes.

With reference to level schemes that is more complex [100] we considered the level $^3H_5$ to be empty due to fast relaxation to $^3F_4$ without losing in precision for our investigation. Below we report the corresponding rate-equation system we used to analyze our experimental data.

$$\frac{dN_0}{dt} = -W_{03}N_0 + \frac{N_3}{\tau_{30}} + \frac{N_1}{\tau_1} - C_R(N_{Tm})N_3N_0 \qquad (3.1)$$

$$\frac{dN_1}{dt} = \frac{N_3}{\tau_{31}} - \frac{N_1}{\tau_1} + 2C_R(N_{Tm})N_3N_0 \qquad (3.2)$$

$$\frac{dN_3}{dt} = W_{03}N_0 - \frac{N_3}{\tau_{30}} - \frac{N_3}{\tau_{31}} - C_R(N_{Tm})N_3N_0 \qquad (3.3)$$

The model includes pump (W_{03}) mechanism, and cross-relaxation mechanism (C_R). Where N_0, N_1, and N_3 are the populations of Tm^{3+} ions in the $^3H_6$, $^3F_4$, and $^3H_4$ levels respectively, W_{03} the pump rate (s^{-1}) and C_R the cross relaxation parameter, the τ_{xy} are the lifetimes of the x to y transition and τ_z is the lifetime of level z. Note that $\tau_3=(\tau_{31}^{-1}+\tau_{30}^{-1})^{-1}$. At steady state the time derivatives in the rate equations are equal to zeros. Considering the conservation law of Tm^{3+} ions populations, we can also write:

$$N_t = N_0 + N_1 + N_3 \qquad (3.4)$$

The pump absorption is given by

$$W_{03} = \sigma_a(\lambda_p)\, F_p N_0 \qquad (3.5)$$

Where $\sigma_a(\lambda_p)$ is the absorption cross section at pump wavelength and F_p is the pump photon flux. The pump photon flux is given by

$$F_p = P_p / h\nu_p \qquad (3.6)$$

Where P_p is the pump power, h is plank constant, and ν_p is pumping frequency.The above rate equations system can be solved using a suitable numerical program.

What is important is now to correlate the parameter of the model with the data we can obtain from experiments. In particular once we measure the lifetime of the level $^3H_4$ we have, Using the above rate equations system of Fig.3.1, the cross-relaxation rate C_RN_0 can be measured using the relation [38] from the measurement of the experimental lifetime of $^3H_4$ level:

$$\frac{1}{\tau_{30}} = \frac{1}{\tau_{31}} + C_R N_0 \quad \text{and therefore} \quad C_R = \frac{1}{N_0}\left(-\frac{1}{\tau_{31}} + \frac{1}{\tau_{30}}\right) \tag{3.7}$$

Where τ_{30} is the measured lifetime of the $^3H_4$ level. The measurement of lifetime of $^3H_4$ can be made by observing the emitted radiation at 1470 nm. However as we will discuss later this requires an experimental set-up with time resolution of the order of 1 μs or below.

An alternative solution is to investigate the steady-state emission of 1470-nm radiation from $^3H_4$ level and the 1800 nm radiation from $^3F_4$ level. By setting all derivatives equal to zero in eq. 3.2 we obtain

$$C_R = \frac{1}{2N_0}\left[-\frac{1}{\tau_{31}} + \frac{N_1}{N_3\tau_1}\right] \tag{3.8}$$

If we now apply the Fuchtbauer-Landenburg rule [101] that related the transition lifetime to emission spectra and emission cross section and the relationship that relates the amount of emitted spontaneous photons to excited ions and emission cross section [102] we find the two general relationships:

$$\sigma_{e,ij}(\lambda_p) = K\frac{\lambda_p^4}{A_{i,j,norm}\, n^2(\lambda_p)\tau_{ij}} \tag{3.9}$$

$$\sigma_{e,ij}(\lambda_p) = H\frac{\Phi_{ij}(\lambda_p)}{N_i\,\Delta\nu} \tag{3.10}$$

Where σ_{ij}, $A_{ij,norm}$, τ_{ij} are the emission cross section, the Area of emission spectrum normalized to the maximum and the transition radiative lifetime; H and K are constant independent from the transition, n the glass refractive index at transition wavelength; Φ_{ij} the number of photons emitted at peak wavelength in a frequency

interval $\Delta\nu$, N_i the excited ion population, and λ_p the wavelength of the peak of emission spectrum. By combining the two equations we finally have:

$$\frac{N_i}{\tau_{ij}} \propto \frac{\Phi_{ij}(\lambda_p)}{\Delta\nu_p \lambda_p^4} A_{ij,norm}\, n^2(\lambda_p) \qquad (3.11)$$

If we now rewrite the Eq.3.8 and we use Eq.3.11 for the 1800 nm and 1470 nm radiation we have:

$$C_R = \frac{1}{2N_0}\left[-\frac{1}{\tau_{31}} + \frac{N_1}{N_3\tau_1}\right] = \frac{1}{2N_0}\left[-\frac{1}{\tau_{31}} + \frac{\tau_{31}N_1}{\tau_{31}N_3\tau_1}\right] =$$
$$= \frac{\beta_{31}}{2N_0\tau_3}\left[\frac{\Delta\nu_{p,31}\Phi_{10}\lambda_{p,31}^4 A_{10,norm} n^2(\lambda_{p,10})}{\Delta\nu_{p,10}\Phi_{31}\lambda_{p,10}^4 A_{31,norm} n^2(\lambda_{p,31})}\frac{\tau_{1,0}}{\tau_1} - 1\right] \qquad (3.12)$$

Where β_{31} is the branching ratio of the 1470 nm transition and $\tau_{1,0}$ is the lifetime of $^3F_4$ for an isolated ion. This formula will be used to calculate the cross relaxation even for highest doped samples where Eq.3.7 fails due to experimental resolutions limits.

3.4 Simulation

To explore the effects of cross-relaxation energy transfer on the population densities of the ions at $^3H_6$, $^3F_4$ and $^3H_4$ levels, simulations have been carried out. To simplify the simulation, a three level system is employed in the model. We assumed a low pumping regime and that the almost Tm^{3+} ions were in the ground state. Fig. 3.2 shows the simulation of the population densities at given CR for 1.08 Tm^{3+} sample.

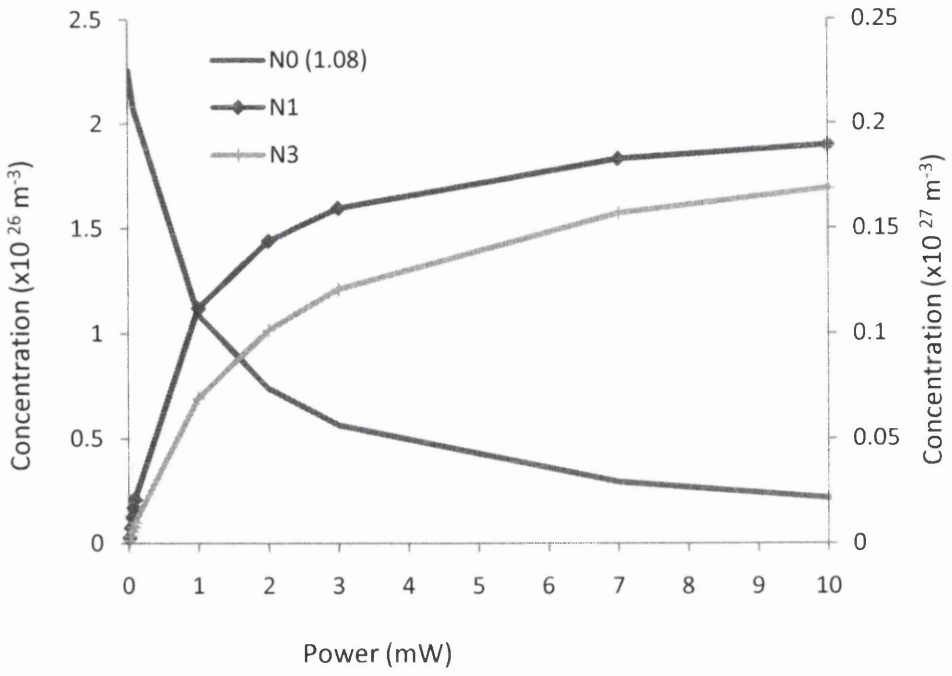

Fig.3.2 Simulation for Tm^{3+} sample with concentration of $2.28x10^{26}m^{-3}$

3.5 Fitting

For well description of the fluorescence from Tm^{3+} ion, matlab program and single exponential fittings to the decay waveform has been conducted. The fittings were applied to the decay from both levels $^3H_4$ and $^3F_4$ to characterise the lifetime values.

The decay curves from $^3F_4$ level exhibit exponential behaviour. As instant, Fig. 3.3 illustrates a matlab program fit to the $^3F_4$ level decay for T1.08 sample.

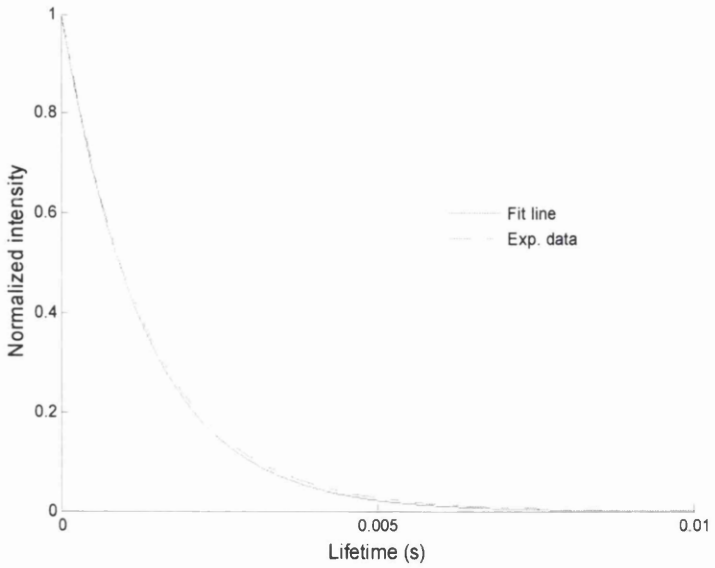

Fig. 3.3 a program fitting to the $^3F_4$ level of T1.08 sample

From Fig. 3.3 it can be concluded that the program fitting succeeds to describe the decay curve for most time.

Chapter 4
Thulium doped tellurite glasses

4.1 Experimental techniques

All samples of bulk TZN tellurite glasses used in our experiments were made with the compositions $75TeO_2$-$20ZnO$-$5Na_2O$ (mol %) and were doped with various amounts of Tm^{3+} concentrations (0.36 wt up to 10 wt %). The employed chemicals and their purities were the following: TeO_2 (99%), ZnO (99,99%), Na_2CO_3(99,995%). In order to minimize the hydroxyl ion (OH) content, which is necessary for achieving good laser performance, glasses were prepared by melt quenching from batches inside a glove box in a dry atmosphere. Fluorescence measurements were conducted, in which Tm^{3+} fluorescence was excited by a laser diode at 785 nm, and emission spectra were observed in bulk glass samples. Lifetime measurements were carried out by modulating the excitation source and fluorescence decays in bulk glass samples were recorded by DSO5034 Agilent Oscilloscope.

Fig. 4.1 displays the experimental setup that was used to pump the Tm^{3+} doped tellurite glass and measure lifetime values.

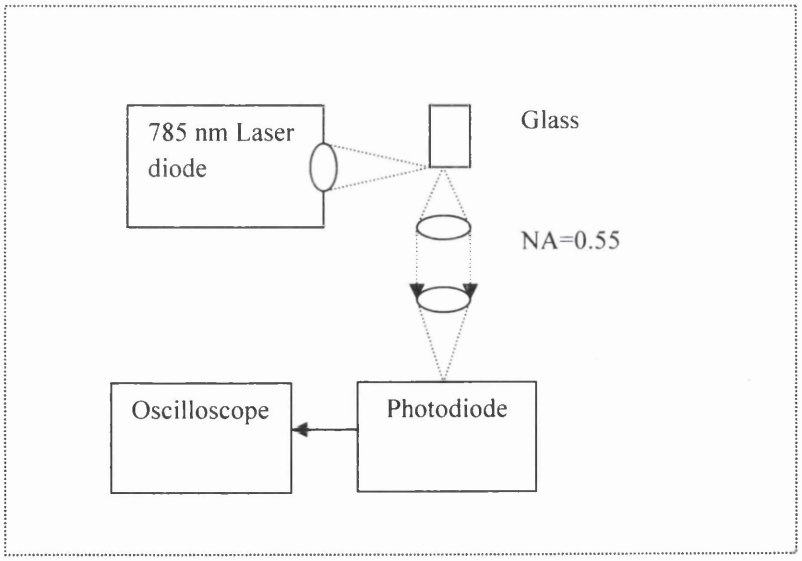

Figure 4.1 Experimental setup

The aim is to measure the absorption and emission spectra of glass samples with different doping concentrations at room temperature.

In order to excite thulium ions, the pump beam from 785 nm laser diode was first collimated and then focused into the glass sample. The beam was focusing in a small area at the edge of the sample to reduce undesired effects of radiation trapping and re-absorption that may alter the measurement. The signal was collected orthogonally with respect to the excited beam, then focused on photodiode using a collimated lens with focal length of F = 20 mm and diameter of D = 18 mm. The collecting lens had a limited numerical aperture. This reduces the signals but also reduce the lifetime measurement errors due to re-absorption. Before photodiode a long-pass filter with cut-off at around 1500 nm was used to measure the $^3F_4$ level lifetime while a 1450 nm pass-band filter was used to measure the $^3H_4$ lifetime. The spectra were recorded by spectrometer covering the 900 nm – 2500 nm wavelength interval (Ocean Optics mod. NIR-256).

To ensure that no self trapping was going to alter the lifetimes and emission spectra measurement we measured lifetimes by focusing the pump on the edge and 1-mm within the samples and we found the same values. For two of the samples, Fig. 4.2(a) shows that no variation had been observed up to 0.6 mm. On the contrary Figure 4.2(b) shows that the emission spectra are affected if we focus within the bulk. In this figure we show the emission spectra of $^3F_4$ radiation of all samples normalized to peak value and with pump focusing on the sample edge (within 0.3 mm from surface) and the spectra of T7 when focused at 0.9 mm. The shift is mainly due to re-absorption of phonons emitted directly from the pumped volume. Instead Fig.4.2 (a) we do not see any effect since re-absorption only decrease the signal but does not alter the lifetime measure.

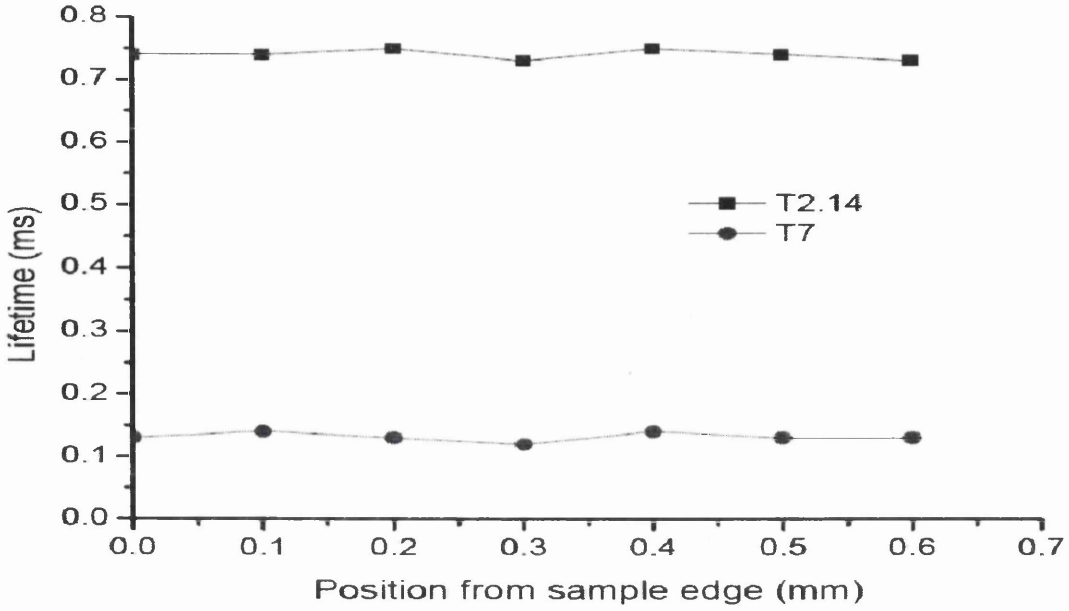

Fig. 4.2(a) Lifetimes of T2 and T7 samples at different positions

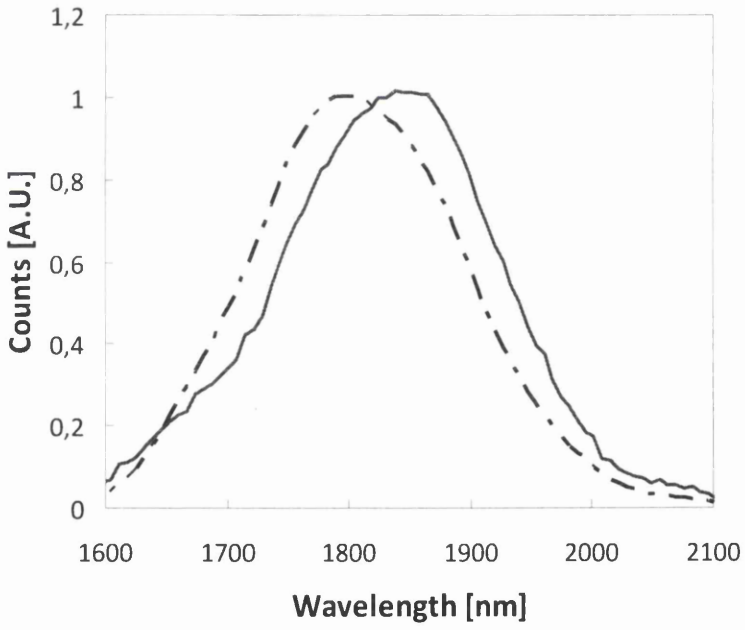

Fig.4.2 (b) Emitted spectra for T7 with pump focused at 0.3 mm (solid line) and 0.9 mm (dashed line) focused from the edge.

4.2 $Tm3^{+}$ spectroscopy in tellurite glass

Samples of Tm-doped tellurite glasses were excited at the wavelength of 785 nm. Two transition bands centred at 1.47 and 1.8 μm, which corresponding to $^3H_4 \rightarrow {}^3F_4$ and $^3F_4 \rightarrow {}^3H_6$ respectively were observed. The infrared emission in the 1300-2200 nm spectra was obtained for given samples. Fig. 4.3 shows the fluorescence spectra corresponding to $^3H_4 \rightarrow {}^3F_4$ and $^3F_4 \rightarrow {}^3H_6$ transitions normalized to $^3H_4 \rightarrow {}^3F_4$ transition. The spectra show a strong emission band centred at 1800 nm and less intense emission band at 1470 nm. The intensity of the emission corresponding to the $^3H_4 \rightarrow {}^3F_4$ strongly decreases with respect to the increasing of the Tm^{3+} concentration. The growth of the intensity of the 1.8 μm in comparison to the 1.47 μm as the Tm^{3+} concentration increased had been previously observed, and this is evidence of the cross-relaxation between both transitions [103,104].

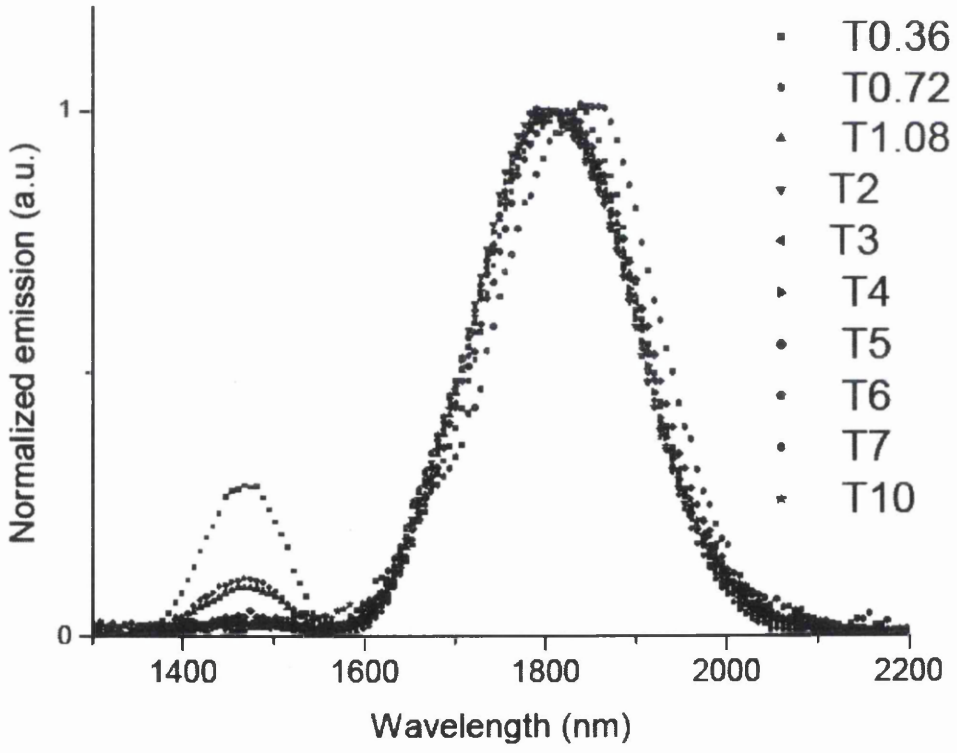

Fig. 4.3 Normalized emission spectra of all samples at 1800 nm

From this scheme as the dopant concentration arises, the intensity of the 1.8 μm band increases in comparison of the 1.47 μm peak. Full width at half maximum (FWHM) of the 1.8 μm band is up to 200 nm, which appears broader than in the case of silica 150 nm [100] and 125 nm in ZBLAN glass [44]. This wide broadening is good for enhancing the turning lasers employing a tellurite glass hosts. Some of the fluorescence bands of the $^3F_4$ level are shifted towards longer wavelength due to re-absorption effects.

Fig. 4.4 illustrates the emission ratio with respect to the Tm^{3+} concentrations. From this figure the relatively increasing in emission of $^3F_4$ manifold with an increase in Tm^{3+} concentration is probably resulting from cross-relaxation between the two transition bands. This ratio could give an insight into the concentration dependence of the efficiency of the CR process. According to dopant concentration, it could be noticed that cross-relaxation process has affect up to 3 mol %. Less $^3H_4$ emission for higher dopant concentration can be observed.

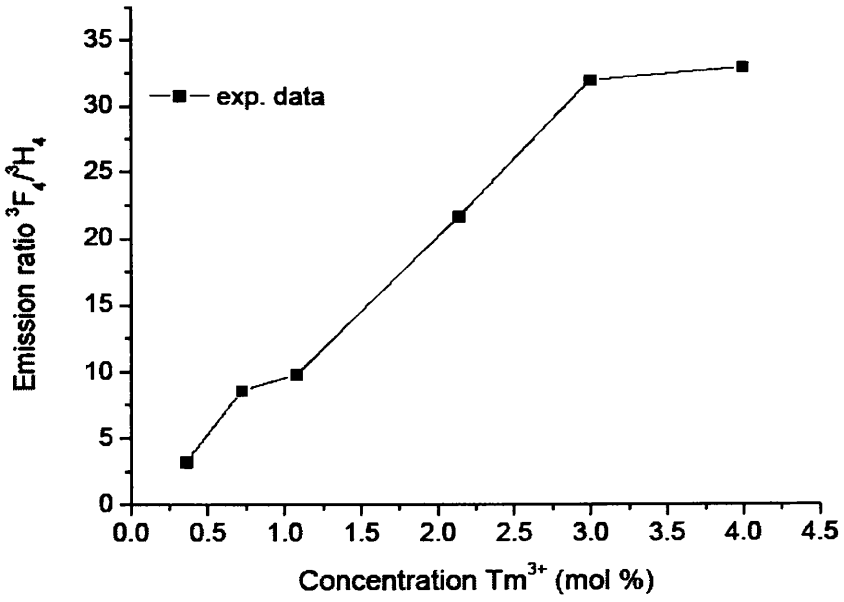

Figure 4.4 Emission ratios between $^3F_4$ and $^3H_4$ bands.

4.2.1 Absorption spectra

Fig. 4.5 shows the absorption transitions for the sample T3 with concentration of 6.84 x 10^{20} cm^{-3} . This figure is characterized by the bands corresponding to the transitions starting from the ground level $^3H_6$ to other higher levels. The transitions were labeled as $^1G_4$, $^3F_3$, $^3H_4$, $^3H_5$ and $^3F_4$.

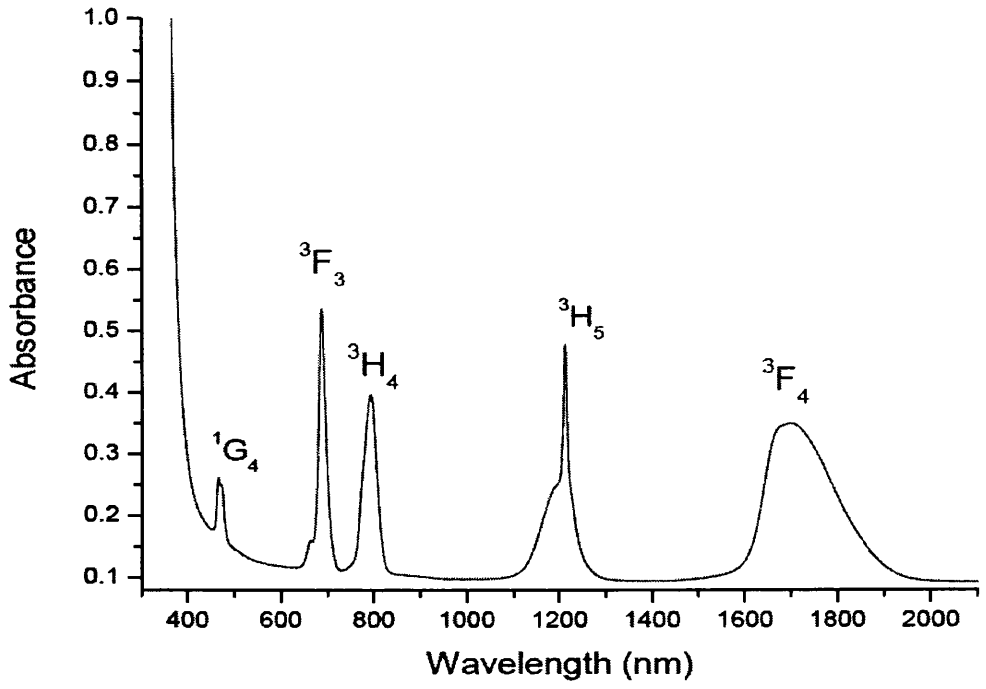

Figure 4.5 Absorption transitions spectrum for sample T3

Absorption coefficient (α) was calculated by using the relation $\alpha = \frac{2.303}{L}$, where L is the sample thickness in cm (samples were used in the measurements have a thickness of 1-2 mm). The absorption spectrum shows the suitability of Tm^{3+} for pumping at ~ 800 nm into the $^3H_4$ level. This feature was employed in Tm^{3+} co-doped Ho^{3+} system, since Ho^{3+} ions do not have any absorption bands close 800 nm for pumping [38]. Fig. 4.6 shows the absorption cross section of the Tm^{3+} doped tellurite bulk glass T3 sample used in this work. The peak absorption cross section value is 6 x 10^{-26} m^2.

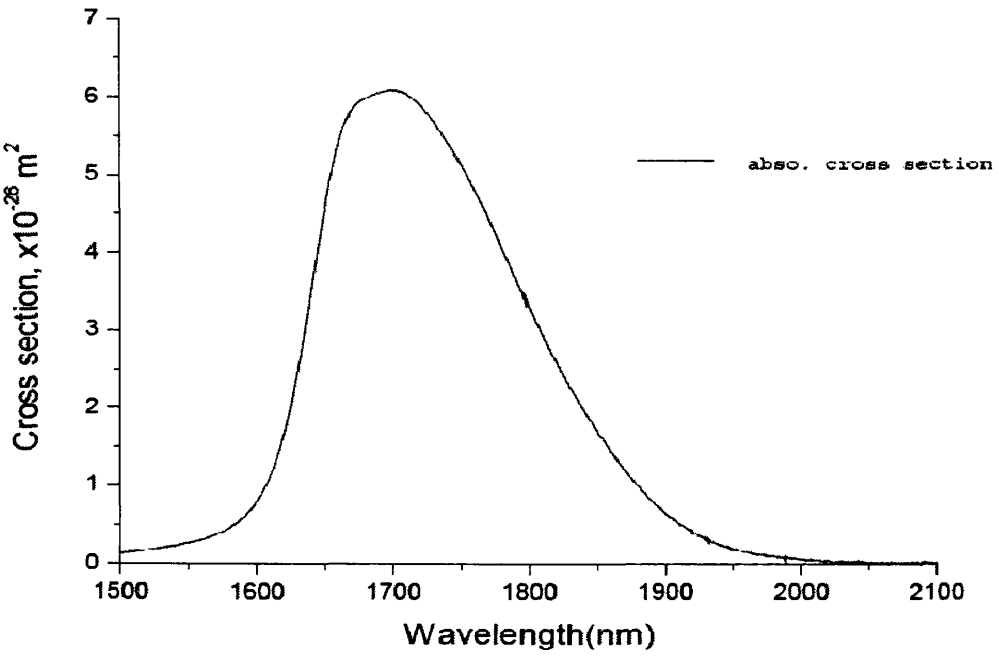

Fig. 4.6 Absorption cross section of Tm^{+3} doped tellurite glass T3 sample.

Two absorption bands $^3H_4$ and $^3F_4$ of the five bands indicated in Fig. 4.5 were chosen for the calculation. The radiative probabilities and the branching ratios of these two brands are shown in Table 1.

Table 1 the spectroscopic properties of Tm^{3+} ions in $75TeO_2$-20ZnO-$5Na_2$

Transition	$\lambda(\mu m)$	$A_{ij}(s^{-1})$	β
$^3F_4 \rightarrow {}^3H_6$	1.8	378.7	1
$^3H_4 \rightarrow {}^3F_4$	1.4	2688.1	0.0762

In the table 1 $A_{ij}(s^{-1})$ is referring to spontaneous radiative transition from (i) level to (j) level and β is branching ratio.

4.2.2 Emission spectra

The emission associated with the Tm^{3+} transition from $^3H_4 \rightarrow {}^3F_4$ covers the spectral range from 1440 to 1520 nm [105]. Hence, Tm^{3+} doped glass could be desirable for S-band optical amplification. Fig. 4.7 shows the normalized emission spectra of Tm^{3+} in T0.36, T0.72, and T1.08 samples. It shows that the spectra have a peak at 1470 nm. From this graph, it is clear that fluorescence becomes broader at higher Tm^{3+} mol %. The full width at half maximum (FWHM) value is about 105 nm. Obviously, the FWHM increases with increasing Tm^{3+} content. The bandwidth properties of the optical amplifier can be evaluated from the product FWHM x σ_e. The larger the product is, the better are the properties of amplifier. The McCumber theory [93] is reported how to calculate the emission cross-section (σ_e).

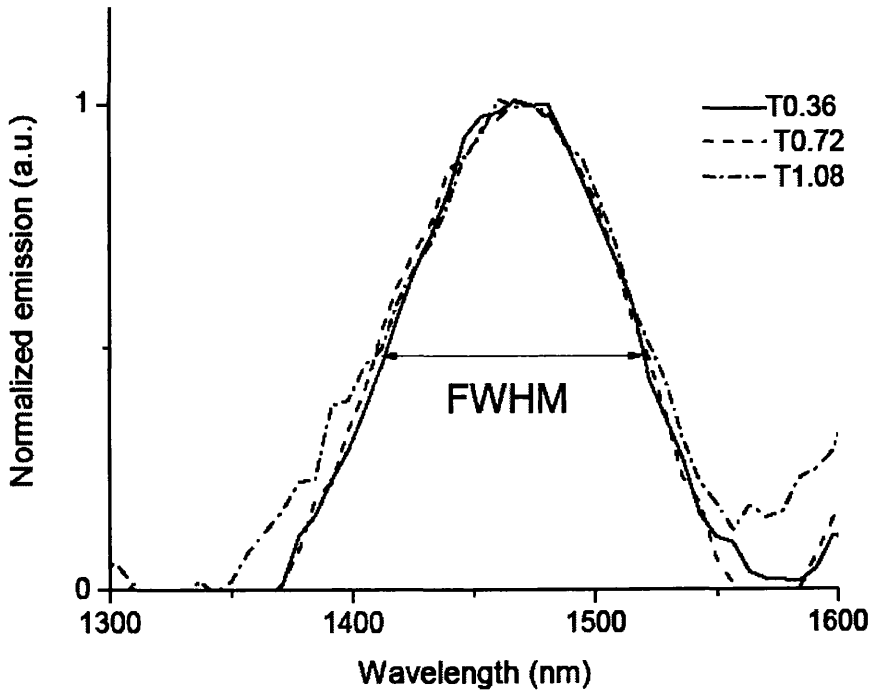

Fig.4.7 Normalised emission spectra of the $^3H_4 \rightarrow {}^3F_4$ transitions

4.2.3 Lifetime measurements

From the theoretical investigation we need to know the lifetime of $^3H_4$ level for all samples to calculate the cross relaxation parameter or, alternatively, the lifetime of $^3F_4$ level and the emission spectra. As shown in Fig. 4.8 the measured Tm^{3+}: $^3F_4$ lifetimes with varying Tm^{3+} concentration showed a significant drop from 2.5 ms in the 0.36 wt % Tm^{3+} sample to 0.07 ms in the 10 wt % sample, where dropping process illustrates the concentration quenching effect. Using the setup-up described in Fig.4.1 we measured the lifetime of $^3H_4$ and $^3F_4$ levels and we fit the experimental lifetime values using the formula proposed by Auzel et al [80]: Lifetime values were calculated for all samples and are reported in Table 2.

$$\tau_i = \frac{\tau_{i,0}}{\left(1 + \frac{9}{2\pi}\left(\frac{N}{N_q}\right)^2\right)} \qquad (4.1)$$

Where τ is the measured lifetime at a given concentration N, $\tau_{1,0}$ is the lifetime for a single isolated ion. The quenching concentration N_q represent the value at which the quenching becomes relevant. Figure 4.8 and Figure 4.9 shows respectively the measured values. The experimental data are in good agreement with the fit curve. The Tm^{3+}: $^3H_4$ lifetime values were difficult to collect in case of high concentration.

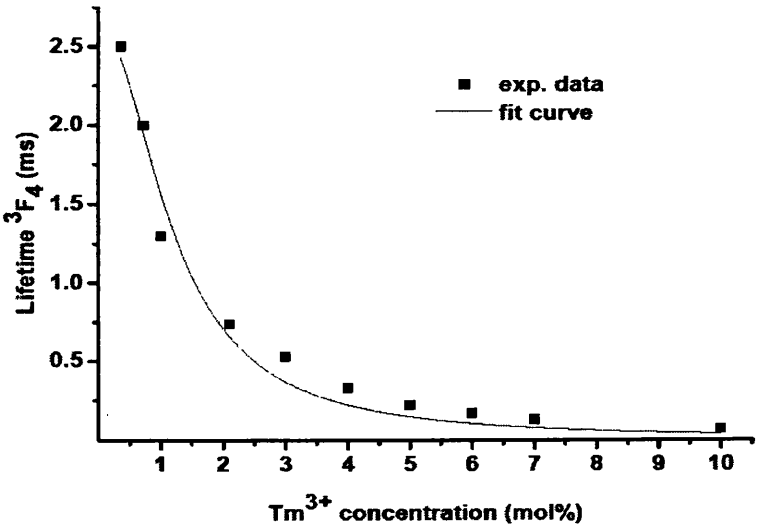

Figure 4.8 Correlation between $^3F_4$ lifetime and Tm^{3+} concentration

Figure 4.9 shows the values of the measured lifetimes of the $^3H_4$ level. In this figure only samples up to 4 mol% were recorded. In fact the speed of the photodiode was limited to microsecond and at the present we were not be able to measure lifetime shorter than that values. The quenching concentration (Nq) for $^3F_4$ level fitted using the formula proposed by Auzel et al was about 1.45 x 10^{20} cm^{-3} while the radiative lifetime (τ_0) was about 2.64 ms. For $^3H_4$ level the Nq was 1.10 x 10^{20} cm^{-3} and the τ_0 was 0.37 ms. For sample T5 and higher concentration the lifetime of $^3H_4$ level was affected by the resolution of our system and we did not consider it a reliable data. However we were able to calculate the C_R for the first six samples.

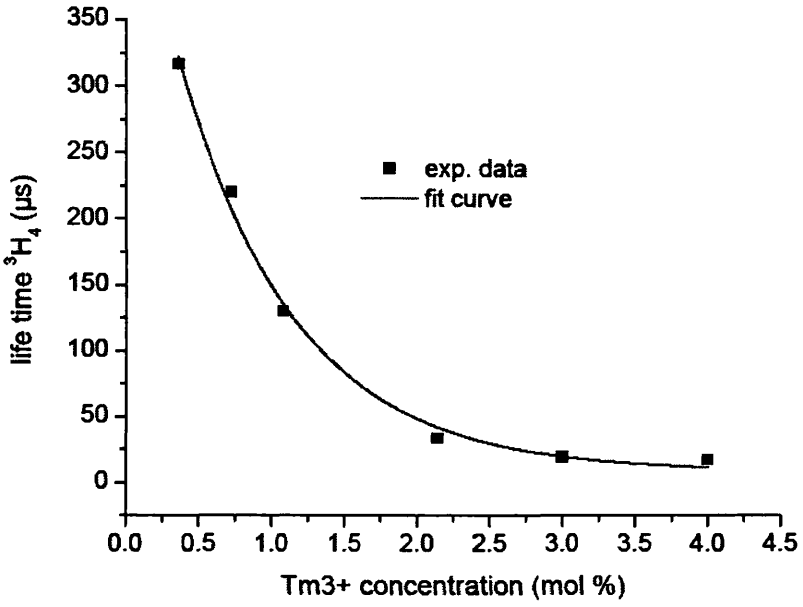

Figure 4.9 Correlation between $^3H_4$ lifetime and Tm^{3+} concentration

Table 2 shows the measured lifetime values. In this table we can see that the lifetime values are decreased with respect to the increasing in dopant concentration. This case is attributed to cross-relaxation process $^3H_4$, $^3H_6 \rightarrow {}^3F_4$, $^3F_4$.

Table 2 Lifetime values of $^3H_4$ and $^3F_4$ levels

Sample	Tm^{3+} $\times 10^{26}m^{-3}$	$^3H_4$ (μs)	$^3F_4$(ms)
T0.36	0.82	317	2.5
T0.72	1.65	220	2
T1.08	2.28	130	1.3
T2.14	4.87	34	0.74
T3	6.84	19.9	0.53
T4	9.06	12	0.33
T5	11.3	-	0.2
T6	13.5	-	0.17
T7	15.7	-	0.13
T10	22.1	-	0.07

4.2.4 Concentration quenching of the $^3H_4$ and $^3F_4$ emission

The concentration dependence of the quenching ratio (R_Q) can be expressed as $R_Q = \frac{1}{\tau_m} - \frac{1}{\tau_0}$, where τ_m is the measured lifetime and τ_0 is the radiative value. A slope equal to two was obtained in Fig. 4.10 which indicates the CR process presents in the case of fast diffusion.

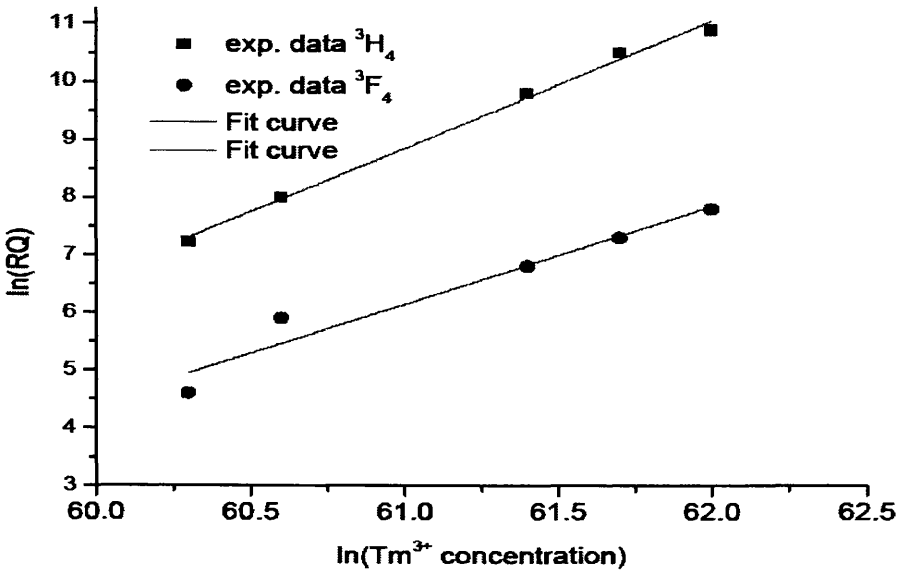

Figure 4.10 Logarithmic dependence of quenching rate and Tm^{3+} concentration.

4.2.5 Cross-relaxation mechanism

The emission of the $^3F_4 \rightarrow {}^3H_6$ band is due to the cross-relaxation process $^3H_4$, $^3H_6 \rightarrow {}^3F_4$, $^3F_4$. This process was showed at Fig. 3.1. As a result of this process, a quantum efficiency of two can be acquired [106]. Two important parameters are connected to cross-relaxation. The first one is the overlap between absorption transition ($^3H_6 \rightarrow {}^3F_4$) and emission transition ($^3H_4 \rightarrow {}^3F_4$). The second parameter is the average distance between two neighboring Tm^{+3} ions. These parameters should be well understood in order to enhance the cross-relaxation process. According to the model system (3.1, 3.2 and 3.3 equations), it is clear that as the thulium concentration increases, the cross-relaxation becomes more powerful parameter. Cross relaxation (C_R) process influences the strength of the luminescence bands. When the Tm^{3+} concentration is high, a Tm^{3+} ion decaying from $^3H_4$ level to $^3F_4$ level gives energy to another Tm^{3+} ion in its ground state and both ions ended in the energy level $^3F_4$. This can lead to a reduction in the intensity of the 1470 nm in relation to the 1800 nm. Therefore, it is important to determine the ratio of active ion concentrations in the development of Tm^{3+} doped glasses applications, where cross relaxation mechanism plays an effective role.

The results of evaluation the C_R parameter and its dependence on Tm^{3+} concentrations are shown in Fig. 4.11. The data present a linear increase with respect to the Tm^{3+} concentrations. From this dependence we can conclude that CR process is the only ET process that affects in the dynamic of the levels.

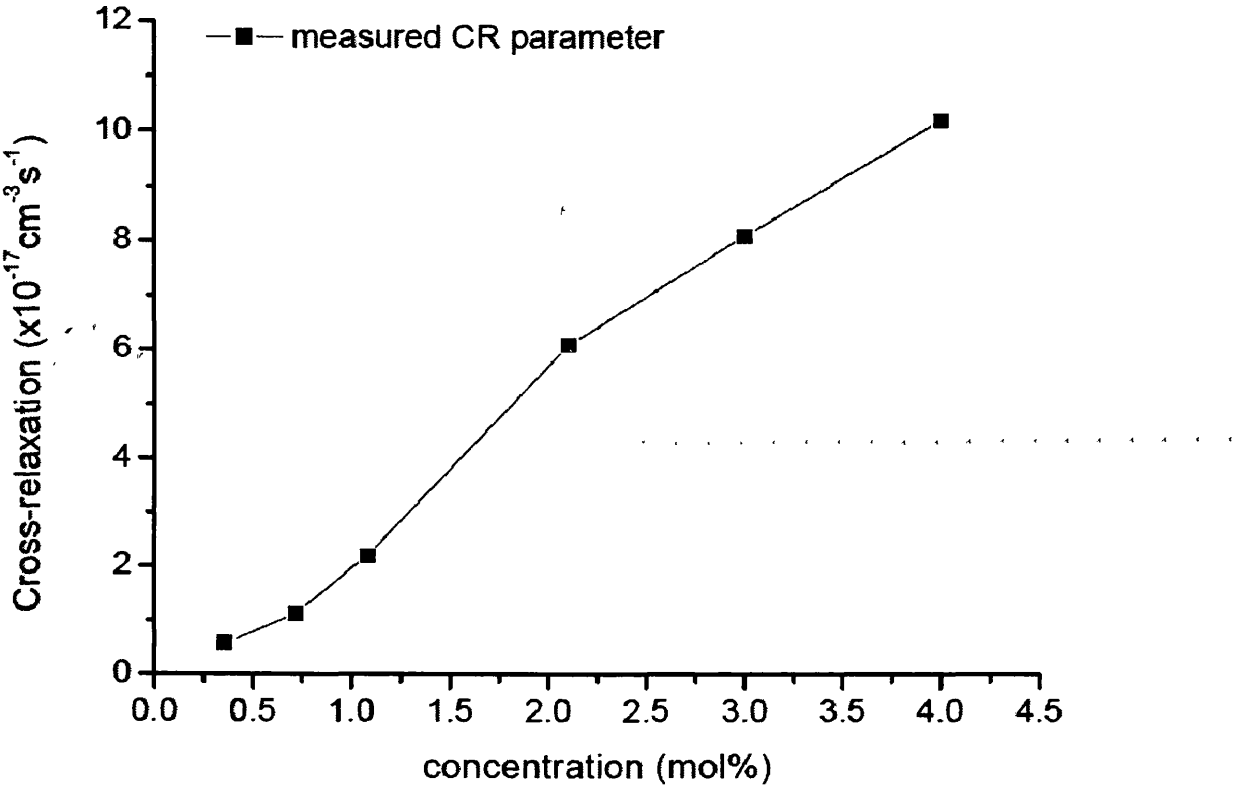

Figure 4.11 Cross-relaxation parameter

Using data from emission spectra and Eq.3.12 we calculate the Cross-relaxation parameter. Since the detector bandwidth was similar at 1470 nm and 1800 nm and the refractive index variation if below 1% we used the following approximated equation:

$$C_R = \frac{\beta_{31}}{2N_0 \tau_3}[kR-1] \qquad (4.2)$$

Where $R=(\Phi_{10}/\Phi_{31})\ (\tau_{1,0}/\tau_1)$ depends on the measures and k contains all other constants $k = (\lambda_{p,10}/\lambda_{p,31})^4\ (A_{10,norm}/A_{31,norm})\ (n^2(\lambda_{p,10})/n^2(\lambda_{p,31}))(\Delta V_{p,31}/\Delta V_{p,10})$. Since

the two peak wavelengths are 1470 nm and 1800 and the normalized area of the $A_{31,norm}$ is half the normalized area $A_{10,norm}$ we have k=1.22. We remind that τ_{31} is the radiative lifetime of the branching ration of 0.076. Where $\tau_{31} = \tau_3 / \beta_{31}$.

Fig. 4.12 shows the values calculated with two approaches. The overlapping until T4 is excellent. In both cases the inversion of the ground level was normalized using the amount of emitted fluorescence under comparable pumping and light collection condition. The fitting shows a linear dependence of C_R from Tm concentration. The data suggest a quite clear linear increase even for highest doped samples.

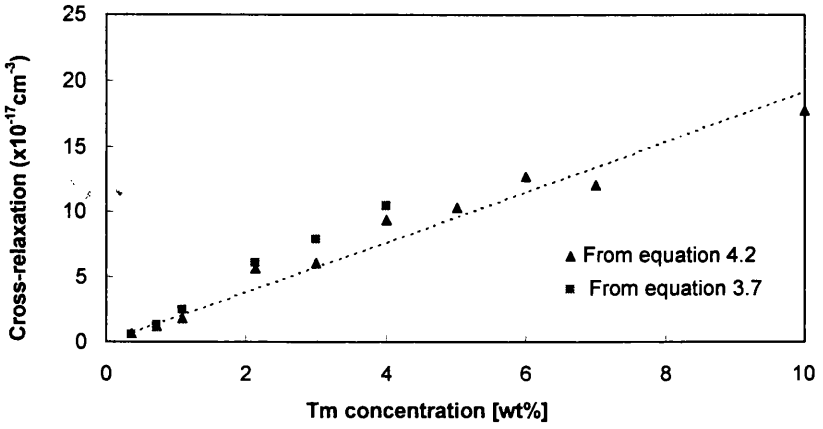

Figure 4.12 Cross-relaxation versus Tm concentration.

In summary the cross-relaxation parameters values for the samples have been evaluated and reported in table 3, where CR1 and CR2 are the cross relaxation parameters resulting from using formulas 3.7 and 3.12 respectively.

Table 3 Cross-relaxation parameters.

Sample	Tm^{3+} ($x10^{20}$ cm^{-3})	CR1 ($x10^{-17}$ $cm^{-3}s^{-1}$)	CR2 ($x10^{-17}$ $cm^{-3}s^{-1}$)
T0.36	0.82	0.56	0.50
T0.72	1.65	1.13	1.00
T1.08	2.28	2.19	1.17
T2.1	4.87	6.11	5. 40
T3	6.84	8.00	5.60
T4	9.06	10.20	8.50
T5	11.3	_	8.70
T6	13.5	_	11.20
T7	15.7	_	11.00
T10	22.1	_	16.10

Chapter 5

CONCLUSION

Spectroscopic investigation of thulium doped tellurite glass ($75TeO_2$-$20ZnO$-$5Na_2O$) has been implemented. The optical properties of an exhaustive series of Tm^{3+} samples from 0.36 wt up to 10 wt have been studied. The main interest on cross-relaxation energy transfer has been considered and the obtained results can reported as below:

Absorption spectrum of given samples were recorded at room temperature. Absorption cross-section for ground state $^3H_6$ from 400 to 2100 nm was obtained. The theoretical discussion of Judd-Oelt theory was reported in the second chapter of this thesis. By using JO theory lifetime and branching ratio values have been calculated.

By using the excited source 785 nm laser diode, emission spectra of bulk glass samples at IR wavelength region have been measured. With respect to the increasing of the concentration level, reduction of 1470 nm fluorescence intensity was showed.

The measured lifetime of $^3F_4$ level drops from 2.5 to 0.07 ms when the Tm^{3+} concentration is increased from 0.36 wt % to 10 wt %, showing the concentration quenching effect. Shifted emission peak of thulium 7 wt % at 1800nm was observed.

The other step of this work involved the study of the exponential fluorescence decay characteristics of both levels $^3H_4$ and $^3F_4$. Two techniques of fitting were applied to the fluorescence decays to obtain the fluorescence lifetime values. The maximum reported lifetimes of the $^3H_4$ and $^3F_4$ levels were 317 μs and 2.5 ms, respectively. The dropping in the $^3H_4$ lifetime from 317 μs to 12 μs was attributed to the cross-relaxation process. Further spectroscopic studies of the Tm^{3+} doped tellurite glasses found the beneficial cross-relaxation process has a remarkable effect on the $^3F_4$ population. The data of cross relaxation parameter in the thulium-doped glasses was found to increase linearly with increasing Tm^{3+} concentration.

To limit re-absorption of the emission from excited Tm^{3+} ions by other neighbor Tm^{3+} ions the pump beam was focused at the sample edge. In case of high Tm^{3+} concentration the re-absorption effect causes in shifted towards lower energy. Utilizing heavily Tm-doped tellurite glasses as active media of short cavity and thus compact fiber lasers is required high Tm^{3+} amount. However, too high amounts can lead to concentration quenching and lifetime shortening, which considered as main factors for reducing quantum efficiency of laser device. The increase in Tm^{3+} content affects the fluorescence properties. Vanishing of 1470 nm emission peaks is due to cross-relaxation process that leads to improving the lasing efficiency at 1810 nm. Fitting curves of lifetime values with respect to the Tm concentrations show a Tm^{3+} concentration quenching.

The intensity of the 1470 nm band was very low, which make measuring $^3H_4$ lifetime so difficult and for high dopant concentration the CR process strongly quenches the emission from the $^3H_4$ level. A critical sensitizer concentration N_0 of magnitude of $(1.45 \pm 0.11) \times 10^{20}$ cm^{-3} and radiative lifetime $\tau_0 = (2.6 \pm 0.1)$ ms are obtained. Finally, the results of calculation the cross relaxation parameter in a range from 0.36 to 4 mol % have been presented and the CR shows a marked linear behaviour.

Publications

1. Milanse D., Gebavi H., Ferraris M., Schulzgen A., Li L., Peyghambarian N. Taccheo S., Taher M., Auzel F., Lousteau J., " Preparation and Characterization of Novel Tm-doped Tellurite Glasses Sensitized with Yb", 8th pacific RIM conference on ceramic and glass technology (Vancouver, Canada) May 31 – June 5, 2009.

2. Taccheo S., Taher M., Milanse D., Gebavi H., Lousteau J., Della Valle G., Barbier D., " Single – frequency waveguide lasers and their design", ICTON 2009 (USA) International Conference On Optical Network 2009 (Island of Sao Miguel, Azores, Portugal) 28/6/2009 – 2/7/2009, DOI: 10.1109/ICTON.2009.5185230

3. D. Milanse, H. Gebavi, Q. Chen, M. Ferraris, M. Taher, S. Taccheo, " Fabrication and characterization of heavily rare-earth doped tellurite glasses for two micron fiber laser", SPIE Photonic West 2009, 7212-3. Optical Components and Materials VI.

4. Gebavi H., Taher M., Lousteau J., Milanse D., Taccheo S., Schulzgen A., Ferraris M., Peyghambarian N., " Spectroscopy of Yb:Tm doped tellurite glasses for efficient infrared fiber laser", The international Society for optical Engineering, SPIE Photonics West (San Francisco) 26-28 January (2010).

5. M. Taher, H. Gebavi, S. Taccheo, D. Milanse, J. Lousteau, A. Schulzgen, M. Ferraris, N. Peyghambarian, " Characterisation of thulium highly doped tellurite glasses for compact fiber lasers", June 28 – July 2, St. Petersburg, Russia, Laser Optics Conference 2010.

6. M. Taher, H. Gebavi, S. Taccheo, J. Lousteau, D. Milanse, N. Peyghambarian, " Lifetime and Cross-relaxation in highly Tm-doped glasses for 2 micron lasers" SPIE 7934, 793407(2011), DOI: 10.1117/12.872848.

7. M. Taher, H. Gebavi, S. Taccheo, D. Milanse, R. Baldas, " Spectroscopy and Investigation of Cross-relaxation in Tm highly-doped glasses " Optics Express Material (2011).

BIBLIOGRAPHY

[1] A. Godard, "Infrared 2-12 μm solid-state laser sources: a review," Comptes Rendus Physique, vol. 8, pp. 1100-1128, 2007.

[2] G. Blackman, "Shooting the breeze," Electro Optics, 2008 / 2009.

[3] S. W. Henderson, C. P. Hale, J. R. Magee, M. J. Kavaya, and A. V. Huffaker, "Eye-safe coherent laser radar system at 2.1 μm using Tm,Ho:YAG lasers," Opt. Lett., vol. 16, pp. 773-775, 1991.

[4] E. V. Browell, S. Ismail, and W. B. Grant, "Differential absorption lidar (DIAL) measurements from air and space," Applied Physics B: Lasers and Optics, vol. 67, pp. 399-410, 1998.

[5] G. J. Koch, B. W. Barnes, M. Petros, J. Y. Beyon, F. Amzajerdian, J. Yu, R. E. Davis, S. Ismail, S. Vay, M. J. Kavaya, and U. N. Singh, "Coherent Differential Absorption Lidar Measurements of CO2," Appl. Opt., vol. 43, pp. 5092-5099, 2004.

[6] S. W. Henderson, P. J. M. Suni, C. P. Hale, S. M. Hannon, J. R. Magee, D. L. Bruns, and E. H. Yuen, "Coherent laser radar at 2 μm using solid-state lasers," Geoscience and Remote Sensing, IEEE Transactions on, vol. 31, pp. 4-15, 1993.

[7] D. Theisen-Kunde, V. Danicke, and R. Brinkmann, "Comparison of two CW Infrared Laser Systems emitting wavelengths at 1.92 μm and 2.01 μm for tissue dissection in liver surgery," vol. 25, 2009, pp. 132-135.

[8] B.M. Walsh, "Review of Tm and Ho Materials, Spectroscopy and Lasers, Laser Physics,," vol. 19, 2009.

[9] Q. Huang, Q. Wang, J. Chang, X. Zhang, Z. Liu, and G. Yu, "Optical parameters and upconversion fluorescence in Tm^{3+}/Yb^{3+} co-doped tellurite glass," Laser Physics, vol. 20, pp. 865-870 (2010).

[10] S. D. Jackson and A. Lauto, "Diode-pumped fiber lasers: A new clinical tool" Lasers in Surgery and Medicine, vol. 30, pp. 184-190 (2002).

[11] J. Y. Allain, M. Monerie, and H. Poignant, "Tunable CW lasing around 0.82, 1.48, 1.88 and 2.35 mu m in thulium-doped fluorozirconate fibre," Electronics Letters, vol. 25, pp. 1660-1662 (1989).

[12] E. R. M. Taylor, L. N. Ng, J. Nilsson, R. Caponi, A. Pagano, M. Potenza, and B. Sordo, "Thulium-doped tellurite fiber amplifier," Photonics Technology Letters, IEEE, vol. 16, pp. 777-779 (2004).

[13] M. Yamane and Y. Asahara, Glasses for photonics (Cambridge: Cambridge University Press, 2004).

[14] A. Jha, S. Shen, and M. Naftaly, "Structural origin of spectral broadening of 1.5-μm emission in Er^{3+} doped tellurite glasses," Physical Review B, vol. 62, p. 6215, 2000.

[15] S. Q. Man, E. Y. B. Pun, and P. S. Chung, "Tellurite glasses for 1.3 μm optical amplifiers," Optics Communications, vol. 168, pp. 369-373, 1999.

[16] S. Shen, A. Jha, L. Huang, and P. Joshi, "980-nm diode-pumped Tm^{3+}/Yb^{3+}-codoped tellurite fiber for S-band amplification," Opt. Lett., vol. 30, pp. 1437-1439, 2005.

[17] A. Mori, T. Sakamoto, K. Kobayashi, K. Shikano, K. Oikawa, K. Hoshino, T. Kanamori, Y. Ohishi, and M. Shimizu, "1.58 - μm Broad-Band Erbium-Doped Tellurite Fiber Amplifier," J. Lightwave Technol., vol. 20, p. 794, 2002.

[18] I. Iparraguirre, J. Azkargorta, J. M. Fernández-Navarro, M. Al-Saleh, J. Fernández, and R. Balda, "Laser action and upconversion of Nd^{3+} in tellurite bulk glass," Journal of Non-Crystalline Solids, vol. 353, pp. 990-992, 2007.

[19] S. Tanabe, K. Hirao, and N. Soga, "Upconversion fluorescences of TeO2- and Ga2O3-based oxide glasses containing Er^{3+}," Journal of Non-Crystalline Solids, vol. 122, pp. 79-82, 1990.

[20] J. S. Wang, D. P. Machewirth, F. Wu, E. Snitzer, and E. M. Vogel, "Neodymium-doped tellurite single-mode fiber laser," Opt. Lett., vol. 19, pp. 1448-1449, 1994.

[21] Y. Ohishi, A. Mori, M. Yamada, H. Ono, Y. Nishida, and K. Oikawa, "Gain characteristics of tellurite-based erbium-doped fiber amplifiers for 1.5-μm broadband amplification," Opt. Lett., vol. 23, pp. 274-276, 1998.

[22] B. Richards, A. Jha, Y. Tsang, D. Binks, J. Lousteau, F. Fusari, A. Lagatsky, C. Brown, and W. Sibbett, "Tellurite glass lasers operating close to 2μ m," Laser Physics Letters, vol. 7, pp. 177-193, 2010.

[23] D. C. Hanna, I. M. Jauncey, R. M. Percival, I. R. Perry, R. G. Smart, P. J. Suni, J. E. Townsend, and A. C. Tropper, "Continuous-wave oscillation of a monomode thulium-doped fibre laser," Electronics Letters, vol. 24, pp. 1222-1223, 1988.

[24] J. E. Shelby "Introduction to Glass Science and Technology", Rcs Paperbacks Series, June 1997.

[25] J. C. McLaughlin, S. L. Tagg, J. W. Zwanziger, D. R. Haeffner, and S. D. Shastri, "The structure of tellurite glass: a combined NMR, neutron diffraction, and X-ray diffraction study," Journal of Non-Crystalline Solids, vol. 274, pp. 1-8, 2000.

[26] D. L. J. Heo, G.H. Sigel "Spectroscopic Analysis of the Structure and Properties of Alkali Tellurite Glasses," Journal of the American Ceramic Society, vol. 75, pp. 277-281, 1992.

[27] M. Zhang, S. Mancini, W. Bresser, and P. Boolchand, "Variation of glass transition temperature, Tg, with average coordination number, ‹m›, in network glasses: evidence of a threshold behavior in the slope dTg/d‹m› at the rigidity percolation threshold (‹m› = 2.4)," Journal of Non-Crystalline Solids, vol. 151, pp. 149-154, 1992.

[28] R. EL-Mallawany, "The optical properties of tellurite glasses," J. Appl. Phys., vol. 72, pp. 1774-1777, 1992.

[29] Y. A. Asahara, Glasses for photonics (cambridge university press), 2000.

[30] E. A. D. Barbier, "Amplifing four-wavelength combainer, based on erbium/ytterbium-doped waveguide amplifiers and integrated splitters," Photonics Technology Letters, IEEE, vol. 9, pp. 315-317, 1997.

[31] M. J. E. Digonnet, Rare - Earth Doped Fiber Lasers And Amplifiers, 2nd. ed. New York: Basel: Marcel Dekker, 2001.

[32] L. Huang, S. Shen, and A. Jha, "Near infrared spectroscopic investigation of Tm^{3+}-Yb^{3+} co-doped tellurite glasses," Journal of Non-Crystalline Solids, vol. 345-346, pp. 349-353, 2004.

[33] K. Arai, H. Namikawa, K. Kumata, T. Honda, Y. Ishii, and T. Handa, "Aluminum or phosphorus co-doping effects on the fluorescence and structural properties of neodymium-doped silica glass," Journal of Applied Physics, vol. 59, pp. 3430-3436, 1986.

[34] V. A. G. Rivera, E. F. Chillcce, E. Rodriguez, C. L. Cesar, and L. C. Barbosa, "Planar waveguides by ion exchange in Er^{3+}-doped tellurite glass," Journal of Non-Crystalline Solids, vol. 352, pp. 363-367, 2006.

[35] H. Gebavi, D. Milanese, G. Liao, Q. Chen, M. Ferraris, M. Ivanda, O. Gamulin, and S. Taccheo, "Spectroscopic investigation and optical characterization of novel highly thulium doped tellurite glasses," Journal of Non-Crystalline Solids, vol. 355, pp. 548-555, 2009.

[36] R. Wu, et al: Fluorescence lifetime and 980 nm Energy transfer Dynamics in Erbium and Ytterbium Co-doped Phosphate laser glasses, Photonics West 2003, SPIE, (2003)

[37] I. A. Grishin, V. A. Gur'ev, E. B. Intyushin, Y. E. Elliev, O. V. Pavlova, and A. P. Savikin, "Magneto-optic and luminescent properties of tellurite glass TeO2-ZnCl doped with rare-earth elements," Russian Journal of Applied Chemistry, vol. 77, pp. 1245-1248, 2004.

[38] G. Chen, Q. Zhang, G. Yang, and Z. Jiang, "Mid-Infrared Emission Characteristic and Energy Transfer of Ho^{3+} Doped Tellurite Glass Sensitized by Tm^{3+}" Journal of Fluorescence, vol. 17, pp. 301-307, 2007.

[39] Y. Gao and et al., "Thermal Stability and Spectroscopic Properties of New Er^{3+}/Yb^{3+} -Codoped Tellurite Glasses," Chinese Physics Letters, vol. 21, p. 1799, 2004.

[40] J. A. Harrington, Infrared fibers and their applications, SPIE Society, 2004.

[41] H. Chen, Y. H. Liu, Y. F. Zhou, and Z. H. Jiang, "Spectroscopic properties of Er^{3+}-doped tellurite glass for 1.55 μm optical amplifier," Journal of Alloys and Compounds, vol. 397, pp. 286-290, 2005.

[42] M. J. Weber, In Handbook on the Physics and chemistry of Rare Earth. North - Holland, Amsterdam, 1979.

[43] W. M. Daud. M.K. Halimah, H.A.A. Sidek, A.W. Zaidan, and A.S. Zainal, "Optical Properties of Ternary Tellurite Glasses, Malaysia," Materials Science - Poland, vol. 28, 2010.

[44] W. Miniscalco, "Optical and Electronic Properties of Rare Earth Ions in Glasses," in Rare-Earth-Doped Fiber Lasers and Amplifiers, Revised and Expanded. vol. null: CRC Press, 2001.

[45] M. G. Mayer, "Rare-Earth and Transuranic Elements," Physical Review, vol. 60, p. 184, 1941.

[46] S. Sudo, Optical Fiber Amplifiers: Materials, Devices, and Applications. Boston: Artech House, Inc., 1997.

[47] P. Urquhart, "Review of rare earth doped fibre lasers and amplifiers," Optoelectronics, IEE Proceedings J, vol. 135, pp. 385-407, 1988.

[48] L. F. Johnson and H. J. Guggenheim, "Infrared-Pumped Visible Laser," Applied Physics Letters, vol. 19, pp. 44-47, 1971.

[49] F. O. Auzel, "Upconversion and Anti-Stokes Processes with f and d Ions in Solids," Chemical Reviews, vol. 104, pp. 139-174, 2003.

[50] D. L. Dexter, "A Theory of Sensitized Luminescence in Solids," The Journal of Chemical Physics, vol. 21, pp. 836-850, 1953.

[51] R. Reisfeld and M. Eyal, "Possible Ways of Relaxations for Excited States of Rare Earth Ions in Amorphous Media," J. Phys. Colloques, vol. 46, pp. C7-349-C7-355, 1985.

[52] W. J. Miniscalco, "Erbium-doped glasses for fiber amplifiers at 1500 nm," Lightwave Technology, Journal of, vol. 9, pp. 234-250, 1991.

[53] J. R. Lakowicz, Principles of fluorescence spectroscopy,. New York: Kluwer Academic/Plenum Publishers, 1999.

[54] M. J. Weber, "Luminescence Decay by Energy Migration and Transfer: Observation of Diffusion-Limited Relaxation," Physical Review B, vol. 4, p. 2932, 1971.

[55] W. E. K. Gibbs, D. J. Booth, and V. K. Bogdanov, "Population dynamics of the $^3F_4$ and $^3H_4$ levels in highly-doped Tm^{3+}: ZBLAN glasses," Journal of Non-Crystalline Solids, vol. 353, pp. 1-5, 2007.

[56] J. P. Robert Hull, R.M. Osgood Jr., Hans Warlimont, Guokui Liu and Bernard Jacquier,, Spectroscopic properties of rare earths in optical materials, Springer series in material science-Up-conversion in RE doped solids vol. 83, 2005.

[57] S. Alphan and et al., "Effect of cross relaxation on the 1470 and 1800 nm emissions in Tm $^{3+}$:TeO 2 -CdCl 2 glass," Journal of Physics: Condensed Matter, vol. 16, p. 2471, 2004.

[58] G. Dominiak-Dzik and et al., "Thulium-doped Ca 4 GdO (BO 3) 3 crystals. An investigation of radiative and non-radiative processes," Journal of Physics: Condensed Matter, vol. 12, p. 5495, 2000.

[59] V. A. French, R. R. Petrin, R. C. Powell, and M. Kokta, "Energy-transfer processes in Y3Al5O12:Tm,Ho," Physical Review B, vol. 46, p. 8018, 1992.

[60] Q. Nie, X. Li, S. Dai, T. Xu, Z. Jin, and X. Zhang, "Energy transfer and upconversion luminescence in Tm^{3+}/Yb^{3+} co-doped lanthanum-zinc-lead-tellurite glasses," Journal of Luminescence, vol. 128, pp. 135-141, 2008.

[61] L. Xu, B. Song, S. Xiao, and J. LÜ, "Up-conversion luminescence of Tm^{3+}/Yb^{3+} co-doped oxy-fluoride glasses," Journal of Rare Earths, vol. 28, pp. 194-197, 2010.

[62] J. Wu, S. Jiang, T. Qiu, M. Morrell, A. Schulzgen, and N. Peyghambarian, "Cross-relaxation energy transfer in Tm $^{3+}$ doped tellurite glass," in Optical Components and Materials II, San Jose, CA, USA, 2005, pp. 152-161.

[63] A. Hayward, W. A. Clarkson, P. W. Turner, J. Nilsson, A. B. Grudinin, and D. Hanna "Efficient cladding-pumped Tm-doped silica fibre laser with high power single mode output at 2μm," Electronics Letters, vol. 36, pp. 711-712, 2000.

[64] S. D. Jackson and S. Mossman, "Efficiency Dependence on the Tm^{3+} and Al^{3+} Concentrations for Tm^{3+}-Doped Silica Double-Clad Fiber Lasers," Appl. Opt., vol. 42, pp. 2702-2707, 2003.

[65] D. A. Simpson, "Spectroscopy of Thulium doped silica glass" Australia: Victoria University, 2005.

[66] F. Guell, J. Gavalda, R. Sole, M. Aguilo, F. Diaz, M. Galan, and J. Massons, "1.48 and 1.84 μm thulium emissions in monoclinic KGd $(WO_4)_2$ single crystals," Journal of Applied Physics, vol. 95, pp. 919-923, 2004.

[67] C. C. Robinson and J. T. Fournier, "Co-ordination of Yb^{3+} in phosphate, silicate, and germanate glasses," Journal of Physics and Chemistry of Solids, vol. 31, pp. 895-904, 1970.

[68] A. Lupei, V. Lupei, A. Ikesue, and C. Gheorghe,"Spectroscopic and energy transfer investigation of Nd/Yb in Y2O3 transparent ceramics," J. Opt. Soc. Am. B, vol. 27, pp. 1002-1010, 2010.

[69] C. Jiang, J. Zhang, P. Deng, G. Huang, H. Mao, and F. Gan, "Optimization of spectroscopic properties of ytterbium-doped laser glasses," Science in China Series E: Technological Sciences, vol. 42, pp. 616-622, 1999.

[70] H. M. Pask, R. J. Carman, D. C. Hanna, A. C. Tropper, C. J. Mackechnie, P. R. Barber, and J. M. Dawes, "Ytterbium-doped silica fiber lasers: versatile sources for the 1-1.2 μm region," , IEEE Journal, vol. 1, pp. 2-13, 1995.

[71] R. Paschotta, J. Nilsson, P. R. Barber, J. E. Caplen, A. C. Tropper, and D. C. Hanna, "Lifetime quenching in Yb doped fibres," Opt. Commun., vol. 136, pp. 375-78, 1997.

[72] D. C. Hanna, R. M. Percival, I. R. Perry, R. G. Smart, and A. C. Tropper, "Efficient operation of an Yb-sensitised Er fibre laser pumped in 0.8 μm region," Electronics Letters, vol. 24, pp. 1068-1069, 1988.

[73] S. G. Grubb, K. W. Bennett, R. S. Cannon, and W. F. Humer, "CW Room-Temperature Blue Upconversion Laser," Opt. Photon. News, vol. 3, pp. 40-40, 1992.

[74] R. G. Smart, D. C. Hanna, A. C. Tropper, S. T. Davey, S. F. Carter, and D. Szebesta, "CW room temperature upconversion lasing at blue, green and red wavelengths in infrared-pumped Pr^{3+}-doped fluoride fibre," Electronics Letters, vol. 27, pp. 1307-1309, 1991.

[75] Q. Jianbei and M. Akio, "Frequency up-conversion luminescence in Yb^{3+} /Ho^{3+} co-doped $Pb_xCd_{1-x}F2$ nano-crystals precipitated transparent oxyfluoride glass-ceramics," Science and Technology of Advanced Materials, vol. 5, p. 313, 2004.

[76] C. Zhao, Q. Zhang, G. Yang, and Z. Jiang, "Laser-diode-excited Blue Upconversion in Tm^{3+}/Yb^{3+}-codoped TeO_2-Ga_2O3-R2O (R=Li, Na, K) Glasses," Journal of Fluorescence, vol. 18, pp. 87-91, 2008.

[77] A. Braud, S. Girard, J. Doualan, M. Thuau, and A. Tkachuk, "Energy-transfer processes in Yb:Tm-doped KY3F10, LiYF4, and BaY2F8 single crystals for laser operation at 1.5 and 2.3 μm," Physical Review B, vol. 61, p. 5280, 2000.

[78] A.E. Siegman, *Lasers*: Mill Valley, CA:Univ.Sci., 1986.

[79] S. Dai, J. Zhang, C. Yu, G. Zhou, G. Wang, and L. Hu, "Effect of hydroxyl groups on nonradiative decay of $Er^{3+}: 4I_{13/2} \rightarrow 4I_{15/2}$ transition in zinc tellurite glasses," Materials Letters, vol. 59, pp. 2333-2336, 2005.

[80] F. Auzel, F. Bonfigli, S. Gagliari, and G. Baldacchini, "The interplay of self-trapping and self-quenching for resonant transitions in solids; role of a cavity," Journal of Luminescence, vol. 94-95, pp. 293-297, 2001.

[81] B. Henderson and G. F. Imbusch, Optical Spectroscopy of Inorganic Solids. Oxford: Clarendon Press, 1989.

[82] T. Miyakawa and D. L. Dexter, "Phonon Sidebands, Multiphonon Relaxation of Excited States, and Phonon-Assisted Energy Transfer between Ions in Solids," Physical Review *B,* vol. 1, p. 2961, 1970.

[83] C. B. Layne, W. H. Lowdermilk, and M. J. Weber, "Multiphonon relaxation of rare-earth ions in oxide glasses," Physical Review B, vol. 16, p. 10, 1977.

[84] M. Ajroud, M. Haouari, H. Ben Ouada, H. Mâaref, A. Brenier, and B. Champagnon, "Study of the spectroscopic properties and infrared-to-visible up-conversion fluorescence of Er^{3+}-doped germanate glasses," physica status solidi (a), vol. 202, pp. 316-329, 2005.

[85] A. Braud, S. Girard, J. L. Doualan, and R. Moncorge, "Spectroscopy and fluorescence dynamics of Tm3+,Tb3+ and Tm3+/Eu3+ doped $LiYF_4$ single crystals for 1.5 μm laser operation," Quantum Electronics, IEEE Journal , vol. 34, pp. 2246-2255, 1998.

[86] S. Q. Man, H. L. Zhang, Y. L. Liu, J. X. Meng, E. Y. B. Pun, and P. S. Chung, "Energy transfer in Pr^{3+}/Yb^{3+} codoped tellurite glasses," Optical Materials, vol. 30, pp. 334-337, 2007.

[87] Y. S. Han, D. J. Lee, and J. Heo, "1.48 μm emission properties and the cross-relaxation mechanism in chalcohalide glass doped with Tm^{3+}," Journal of Non-Crystalline Solids, vol. 321, pp. 210-216, 2003.

[88] L. Zhang and H. Hu, "Evaluation of spectroscopic properties of Yb^{3+} in tetraphosphate glass," Journal of Non-Crystalline Solids, vol. 292, pp. 108-114, 2001.

[89] A. Camargo, I. Terra, L. Nunes, and M. Li , "Energy transfer processes in Yb^{3+} /Tm^{3+} co-doped sodium alumino-phosphate glasses with improved 1.8 μm emission," Journal of Physics: Condensed Matter, vol. 20, p. 255240, 2008.

[90] B. Aull and H. Jenssen, "Vibronic interactions in Nd: YAG resulting in nonreciprocity of absorption and stimulated emission cross sections," Quantum Electronics, IEEE Journal, vol. 18, pp. 925-930, 1982.

[91] R. M. Martin, "Reciprocity between emission and absorption for rare earth ions in glass." vol. Ph.D Worcester: Worcester Poly. Inst., 2006.

[92] B. J. Ainslie, S. P. Craig, and S. T. Davey, "The absorption and fluorescence spectra of rare earth ions in silica-based monomode fiber," Lightwave Technology, Journal , vol. 6, pp. 287-293, 1988.

[93] D. E. McCumber, "Einstein Relations Connecting Broadband Emission and Absorption Spectra," Physical Review, vol. 136, p. A954, 1964.

[94] R. M. Martin and R. S. Quimby, "Experimental evidence of the validity of the McCumber theory relating emission and absorption for rare-earth glasses," J. Opt. Soc. Am. B, vol. 23, pp. 1770-1775, 2006.

[95] B. R. Judd, "Optical Absorption Intensities of Rare-Earth Ions," Physical Review, vol. 127, p. 750, 1962.

[96] G. S. Ofelt, "Intensities of Crystal Spectra of Rare-Earth Ions," The Journal of Chemical Physics, vol. 37, pp. 511-520, 1962.

[97] C. Evans, Z. Ikonic, B. Richards, P. Harrison, and A. Jha,"Theoretical Modeling of a ~2 μm Tm3+-doped tellurite fiber laser : The influence of Cross Relaxation," IEEE, vol. 27, pp. 4026-4032, 2009.

[98] K S Kravtso, I. Bufetov, O. Medvedkov, E.Dianov. M. Yashkov, and A. Guryanov, "7-W single-mode thulium - doped fiber laser pumped at 1230 nm " Quantum Electronics, vol. 35 (7), pp. 586 - 590, 2005.

[99] B. Richards, Y. Tsang, D. Binks, J. Lousteau, and A. Jha, "Efficient ~2 μm Tm^{3+}-doped tellurite fiber laser," Opt. Lett., vol. 33, pp. 402-404, 2008.

[100] S. D. Jackson and T. A. King, "Theoretical Modeling of Tm-Doped Silica Fiber Lasers," J. Lightwave Technol., vol. 17, p. 948 (1999).

[101] C. R. Giles, C. A. Burrus, D. DiGiovanni, N. K. Dutta, and G. Raybon, "Characterization of erbium-doped fibers and application to modeling 980-nm and 1480-nm pumped amplifiers", IEEE Photon. Technol. Lett., vol. 3, no. 4, pp. 363 - 365, 1991.

[102] C. R. Giles and E. Desurvire, "Propagation of signal and noise in concatenated erbium-doped fiber optical amplifiers", J. Lightwave Technol., vol. 9, pp. 147 - 154, 1991.

[103] J.S. Wang, E.M. Vogel, and E. Snitzer, "Tellurite glass: a new candidate for fiber devices," Opt. Mater. vol. 3, 187-203 (1994).

[104] A. Brenier, C. Pedrini, B. Moine, J. Adam, and C. Pledel, " Fluorescence mechanisms in Tm^{3+} singly doped and Tm^{3+}, Ho^{3+} doubly doped indium-based fluoride glasses,"Phys. Rev. B41, 5364-5371(1990).

[105] M. Naftaly, S. Shen, and A. Jha, " Tm^{3+} doped tellurite glasse for a brodband amplifier at 1.47 μm " Appl. Opt, 39, 4979-4984 , 2000.

[106] W. Jianfeng, J. Shibin, L. Tao, G. Jihong, N. Peyghambarian, and N. P. Barnes, "Efficient thulium-doped 2 μm germanate fiber laser," Photonics Technology Letters, IEEE, vol. 18, pp. 334-336 (2006).